Palaeogeography, Palaeoclimatology, Palaeoecology 682 (2026) 113423

Contents lists available at ScienceDirect

Palaeogeography, Palaeoclimatology, Palaeoecology

journal homepage: www.elsevier.com/locate/palaeo

Chronostratigraphical ranges of Lower Jurassic larger benthic foraminifera and lithiotid bivalves calibrated by carbon and strontium isotope stratigraphy (Southern Alps, Italy)

Renato Posenato [a], Davide Bassi [a,*], Mariano Parente [b], Hideko Takayanagi [c,d], Anna Cipriani [e,f], Claudio Garbelli [g], Andrea Montanaro [b,h], Yoshihiro Asahara [i], Yasufumi Iryu [c,d]

[a] Dipartimento di Fisica e Scienze della Terra, Università di Ferrara, via Saragat 1, 44122 Ferrara, Italy
[b] Dipartimento di Scienze della Terra, dell'Ambiente e delle Risorse, Università degli Studi di Napoli Federico II, via vicinale cupa Cintia 21, 80126 Naples, Italy
[c] Department of Earth Science, Graduate School of Science, Tohoku University, Aobayama, Sendai 980-8578, Japan
[d] Advanced Institute for Marine Ecosystem Change (WPI-AIMEC), Tohoku University, Sendai 980-8578, Japan
[e] Department of Chemical and Geological Sciences, University of Modena and Reggio Emilia, Via Campi 103, 41125 Modena, Italy
[f] Lamont Doherty Earth Observatory of Columbia University, 61 Route 9W, 10964 Palisades, NY, USA
[g] Dipartimento di Scienze della Terra, Università 'La Sapienza', P.le A. Moro 5, 00185 Rome, Italy
[h] SOCOTEC Italia, Via Annibale Zucchini 69, 44122 Ferrara, Italy
[i] Department of Earth and Planetary Sciences, Graduate School of Environmental Studies, Nagoya University, Furo-cho, Chikusa, Nagoya 464-8602, Japan

ARTICLE INFO

Editor: Professor L Angiolini

Keywords:
Early Jurassic
Carbonate platforms
Larger benthic foraminifera
Lithiotid bivalves
Strontium isotope stratigraphy
Northern Italy

ABSTRACT

Following the end-Triassic biotic crisis, the first larger benthic foraminifera (LBF) emerged in shallow-water carbonate platforms of the Early Jurassic Tethys, during the Hettangian and Sinemurian. In inner-platform settings, these LBF frequently coexisted with large aberrant bivalves of the *Lithiotis* Facies, characterized by thick, gregarious accumulations. This study re-assesses the biostratigraphy of LBF and lithiotid bivalve faunas in a c. 200 m-thick Pliensbachian shallow-water sedimentary succession of the Rotzo Formation in the Trento Platform (Southern Alps, Italy). By integrating carbon and strontium isotope stratigraphy, we refine the chronostratigraphical framework for key LBF taxa that are widely used in Lower Jurassic carbonate platform biostratigraphy. Strontium isotope stratigraphy reveals that *Orbitopsella primaeva* first occurs in the lowermost Pliensbachian Jamesoni Zone, younger than the late Sinemurian age typically cited. Similarly, the last occurrence of *Orbitopsella praecursor* is in the lowermost upper Pliensbachian (early Margaritatus Zone), later than the traditionally accepted uppermost lower Pliensbachian. This study also constrains the timing of the appearance, development and demise of lithiotid bivalve associations in the Trento Platform. *Lithioperna* first appears in the lowermost Pliensbachian Jamesoni Zone, followed by *Opisoma* near the boundary between the Jamesoni and Ibex zones. Higher in the succession, *Lithiotis* becomes prominent near the Davoei–Margaritatus zone boundary, forming thick accumulations intercalated with brachiopod-rich beds. The final phase of the *Lithiotis* Facies is marked by *Cochlearites–Lithioperna* mounds, starting from the Subnodosus Subzone of the Margaritatus Zone. The disappearance of the lithiotid bivalves coincides with the onset of relatively deeper water conditions at the Rotzo Formation–Misone Limestone boundary in the uppermost Pliensbachian Spinatum Zone.

1. Introduction

Following the Late Permian and end-Triassic mass extinctions, the Early Jurassic documented the recovery and diversification of larger benthic foraminifera (LBF) (BouDagher-Fadel, 2018; Septfontaine, 2020; Simmons, 2020). After the end-Triassic biotic crisis (e.g., Schoepfer et al., 2022), the first LBF forms with microgranular wall texture and complex shell structures appeared in the Hettangian–Sinemurian shallow-water Tethyan carbonate platforms (e.g., Hottinger, 1967; Septfontaine, 1981; Bassoullet, 1997; BouDagher-Fadel and Lord, 2002; BouDagher-Fadel, 2018; Septfontaine, 2020). These early LBF, predominantly polyphyletic lituolid taxa (order

* Corresponding author.
E-mail address: bsd@unife.it (D. Bassi).

https://doi.org/10.1016/j.palaeo.2025.113423
Received 21 February 2025; Received in revised form 10 November 2025; Accepted 11 November 2025
Available online 12 November 2025

Lituolida Lankester, 1885), became important biotic components of Mesozoic Tethyan sedimentary successions.

In inner-platform settings, lituolids were often associated with large bivalves constituting the *Lithiotis* Facies, which formed thick accumulations of gregarious and thick-shelled bivalves that contributed significantly to sedimentary deposits throughout the tropical Tethyan and Panthalassa margins (e.g., Broglio Loriga and Neri, 1976; Geyer, 1977; Chinzei, 1982; Fraser et al., 2004; Posenato and Masetti, 2012; Bassi et al., 2015; Posenato et al., 2018). Among the most distinctive and abundant lithiotid bivalves, the aberrant, extremely elongated or strongly flattened species *Cochlearites loppianus*, *Lithioperna scutata*, and *Lithiotis problematica* proliferated during the Pliensbachian–early Toarcian (Fraser et al., 2004; Posenato and Masetti, 2012; Posenato et al., 2018; Brandolese et al., 2019). The *Lithiotis* Facies contains other gregarious and thick-shelled bivalves, with a long stratigraphical distribution ranging from the Sinemurian to the Late Jurassic. They are represented by the Myalinida *Pseudopachymytilus,* the Ostreida *Gervilleioperna* and *Pachygervillia,* the Carditida *Opisoma,* and the Megalodontida *Pachyrisma* and *Protodiceras* (e.g., Fraser et al., 2004; Posenato et al., 2024). However, identifying these bivalves in the field is challenging due to their random orientations within hard-cemented limestones. Accurate taxonomic classification requires well oriented shell sections showing the diagnostic features (e.g., Berti Cavicchi et al., 1971; Chinzei, 1982; Posenato and Masetti, 2012), highlighting the need for careful reassessment of their reported geographical and stratigraphical distributions.

The rich benthic assemblages of lituolid LBF and lithiotid bivalves flourished after the global negative carbon-isotope excursion (CIE), known as the Sinemurian–Pliensbachian boundary event (e.g., Jenkyns and Clayton, 1986; Hesselbo et al., 2007; Korte and Hesselbo, 2011; Franceschi et al., 2014; Nieto et al., 2023). Stratigraphical correlations suggest that environmental and climatic perturbations associated with this event affected the microbially dominated carbonate platforms in the western Tethyan margins, facilitating the spread of lithiotid faunas (Franceschi et al., 2014, 2019).

During the Pliensbachian, these assemblages thrived in the Trento Platform (Southern Alps), a highly variable lagoonal palaeoecosystem with a complex mosaic of habitats (Bosellini and Broglio Loriga, 1971; Clari, 1975; Posenato and Masetti, 2012; Posenato et al., 2013a, 2013b; Bassi et al., 2015). Their disappearance toward the end of the Pliensbachian (Fugagnoli, 2004; Posenato et al., 2024) reflects broader extinction dynamics: lituolid LBF (i.e., *Lituosepta, Orbitopsella, Palaeomayncina*) became extinct close to the Pliensbachian–Toarcian across the entire Tethyan Realm (e.g., Bassoullet et al., 1985; Bassoullet, 1997; BouDagher-Fadel and Bosence, 2007; BouDagher-Fadel, 2018; Septfontaine et al., 1991; Septfontaine, 2020), whereas a few lithiotid bivalves survived after the early Toarcian marine ecosystem crisis (Posenato et al., 2024).

Although several biostratigraphical schemes for the Lower Jurassic LBF have been proposed (e.g., Septfontaine, 1984; Septfontaine et al., 1991; Bassoullet, 1997; Velić, 2007; BouDagher-Fadel, 2018; Hughes, 2018), their chronostratigraphical calibration remains uncertain.

This study investigates the biostratigraphy of LBF and lithiotid bivalves in a c. 200 m-thick Pliensbachian succession of the Trento Platform. By integrating biostratigraphical data with high-resolution carbon ($\delta^{13}C$) and strontium isotope ($^{87}Sr/^{86}Sr$) stratigraphy, we aim to: (1) reassess the chronostratigraphical age of the key lituolid genus *Orbitopsella*, and (2) constrain the age of the onset, development and demise of the bivalve associations of the *Lithiotis* Facies in the Trento Platform.

2. Lower Jurassic LBF biozones and their chronostratigraphical calibration: historical background

Lituolid LBF were first used for the biozonation of Lower Jurassic carbonate platforms in the southern Apennines of Italy (Sartoni and Crescenti, 1962; De Castro, 1962). However, the High Atlas of Morocco has since become the classical reference area for the micropalaeontology and biostratigraphy of Lower Jurassic LBF (Hottinger, 1967; Septfontaine, 1984). There, six biozones have been distinguished (Septfontaine, 1984): "*Siphovalvulina*" and *Mesoendothyra* zone (lower–middle Sinemurian), *Lituosepta recoarensis* zone (upper Sinemurian), *Orbitopsella* zone (upper Sinemurian–lower Pliensbachian), "*Mayncina*" *termieri* and "*Lituosepta*" *compressa* zone (lowermost upper Pliensbachian), and *Pseudocyclammina liasica* zone (uppermost Pliensbachian).

Correlating these LBF biozones with the ammonite biozones, the backbone of the Lower Jurassic chronostratigraphy, remains challenging due to the rare occurrence of ammonites in shallow-water carbonate deposits (Septfontaine, 1984; Septfontaine et al., 1991; Bassoullet, 1997). The following section reviews the available data for the most stratigraphically significant lituolid LBF species.

Although the first occurrence (FO) and last occurrence (LO) of *Orbitopsella primaeva* have never been directly tied to ammonites, a late Sinemurian–early Pliensbachian age was proposed for this species by Septfontaine (1984, fig. 4, p. 221) based on indirect correlation with ammonite-bearing beds. This interpretation has been widely adopted (e.g., Kabal and Tasli, 2003; BouDagher-Fadel and Bosence, 2007; Velić, 2007; Gale, 2014). In terms of ammonite biozones, the range of *O. primaeva* is generally placed within the Raricostatum–Jamesoni–Ibex zones (Sevillano et al., 2020).

In the High and Middle Atlas, the FO of *Orbitopsella praecursor* has been found above beds containing middle lower-Pliensbachian ammonites of the genus *Tropidoceras*, while its LO below ammonites of the upper lower-Pliensbachian–lower upper-Pliensbachian genus *Fuciniceras* (Septfontaine, 1984; Bassoullet et al., 1999). Based on these findings, the range of *Orbitopsella praecursor* was dated to the uppermost lower Pliensbachian (upper Carixian in Septfontaine, 1984, fig. 4; Septfontaine, 2020) and can be correlated to the upper part of the Ibex and to the Davoei zones. A lower Pliensbachian age also has been documented for *Orbitopsella praecursor* in the central Subbetic Chain (SE Spain; Gonzáles-Donoso et al., 1974, 1977), in Mallorca (Álvaro et al., 1989), and other Mediterranean areas (e.g., Kabal and Tasli, 2003; Velić, 2007). Often associated with *Orbitopsella praecursor*, *Orbitopsella dubari* occurs in the lowermost upper Pliensbachian of Morocco and Algeria (Hottinger, 1967; Bassoullet and Fares, 1969; Bassoullet, 1997), and central Apennines (Chiocchini and Mancinelli, 1977).

The demise of the genus *Orbitopsella* has been mostly placed in the uppermost lower Pliensbachian (Septfontaine, 1984; Bassoullet, 1997; BouDagher-Fadel and Lord, 2002; Septfontaine, 2020). Its persistence up to the end of the Toarcian (BouDagher-Fadel, 2018, fig. 4.11) requires further confirmation. In the central Subbetic Zone (SE Spain), *O. praecursor* disappears from beds bearing early lower-Pliensbachian ammonites (Gonzáles-Donoso et al., 1977, p. 255). However, this finding is related to the drowning of the platform, which occurred during the Ibex Zone (Ruiz-Ortiz et al., 2004) and resulted in the sudden disappearance of *Orbitopsella* in the area. In the Trento platform, the presence of a single specimen of *Protogrammoceras isseli* trans. *marianii* alongside *O. praecursor* suggests that the genus *Orbitopsella* may have persisted into the middle Stokesi Subzone of the lower Margaritatus Zone (lower part of the upper Pliensbachian; Sarti and Ferrari, 1999; Fig. 1).

Other Lower Jurassic LBF species have a longer stratigraphical distribution than *Orbitopsella primaeva* and *O. praecursor*. *Lituosepta recoarensis*, formerly considered an index species for the upper Sinemurian (Septfontaine, 1984; Bassoullet, 1997; BouDagher-Fadel, 2018; Sevillano et al., 2020), actually spans the upper Sinemurian–Toarcian interval (Fugagnoli and Bassi, 2015). *Pseudocyclammina liasica* has been reported from the Hettangian to the lower Toarcian (e.g., Bassoullet, 1997; Septfontaine et al., 1991; Dozet, 2009; BouDagher-Fadel, 2018; Han et al., 2022). *Cymbriaella lorigae* spans from the Hettangian to the Aalenian (Fugagnoli, 1999; Schlagintweit and Velić, 2011; Velić, 2007). *Everticyclammina praevirguliana* has been recorded from the middle Sinemurian to the upper Aalenian (Fugagnoli, 2000; Velić, 2007;

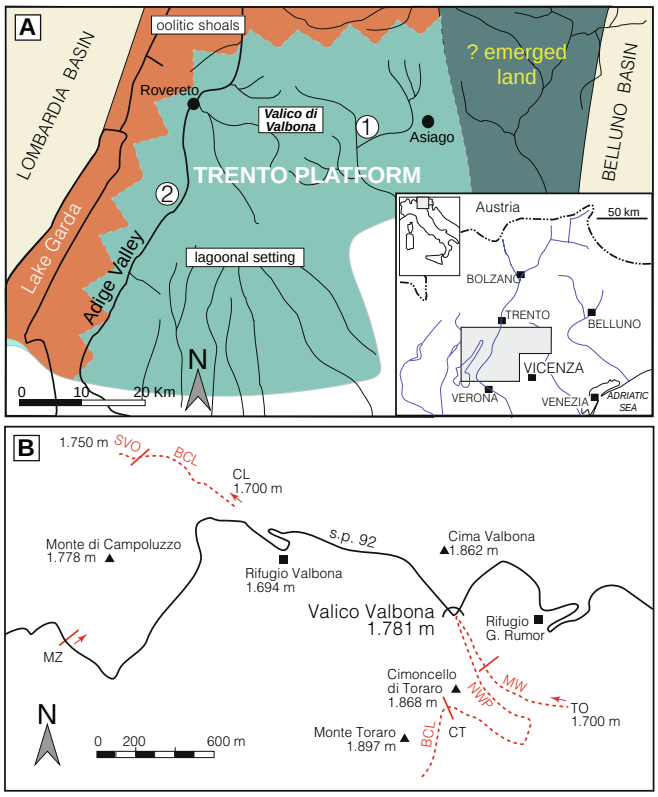

Fig. 1. Geographical location of the studied area. A, the Trento Platform was a Lower Jurassic carbonate platform-plateau of the western Tethyan margin (modified from Posenato and Masetti, 2012). B, the studied succession, located in Valico di Valbona area, was logged in three sections cropping out near Malga Zonta (MZ), along the eastern side of Monte Toraro (TO) and the northeastern side of Monte di Campoluzzo (CL). Arrows point to the stratigraphical top (younging direction). BCL, biocalcarenites with *Cochlearites* and *Lithioperna* accumulations (Rotzo Formation) and Misone Limestone. MW, mudstone-wackestone and marl alternations (Rotzo Formation); NWP, nodular wackestone-packstone and marl alternations (Rotzo Formation); SVO, San Vigilio Oolite; 1, Rotzo type section; 2, Monte Vignola (Sarti and Ferrari, 1999).

Schlagintweit and Velić, 2011; BouDagher-Fadel, 2018) and *Paleomayncina termieri* in the uppermost Sinemurian–Pliensbachian (Bassoullet, 1997; Velić, 2007; BouDagher-Fadel, 2018). *Amijiella amiji* has been reported from the uppermost Sinemurian to the Bathonian (Hottinger, 1967; Schlagintweit, 1991; Fugagnoli, 2004; BouDagher-Fadel, 2018). As no associated ammonite has been found (Han et al., 2022), the stratigraphical correlation of *Bosniella oenensis* to the Ibex Zone requires further confirmation.

3. Stratigraphical setting

In the study area, the Jurassic succession is c. 600 m-thick and consists of shallow-water limestones of the Calcari Grigi Group (Hettangian–Pliensbachian) and the San Vigilio Oolite (Toarcian–lower Aalenian), overlain by the pelagic limestone of the Rosso Ammonitico Veronese (upper Bajocian–Kimmeridgian; Castellarin et al., 2005; Martire et al., 2006). The former two units deposited on a carbonate platform-plateau (Trento Platform), whereas Rosso Ammonitico Veronese is a pelagic nodular limestone recording the drowning of the platform (e.g., Winterer and Bosellini, 1981). The Calcari Grigi Group comprises, in stratigraphical order, the Monte Zugna Formation, the Loppio Oolitic Limestone, the Rotzo Formation, and the Misone Limestone. Unconformity surfaces occur between the Loppio Oolitic Limestone and the Rotzo Formation, between the Misone Limestone and the San Vigilio Oolite, and between the San Vigilio Oolite and the Rosso Ammonitico Veronese (e.g., Masetti et al., 1998, 2012; Castellarin et al., 2005; Martire et al., 2006). The present study focuses on these units.

The Loppio Oolitic Limestone consists mainly of massive oolitic grainstone bodies (35 m-thick in the Rotzo type section; Bosellini and Broglio Loriga, 1971). These deposits accumulated near or within the fair-weather wave base (Masetti et al., 1998; Preto et al., 2017). The upper part is characterized by levels of reddish limestone and bed surfaces with dinosaur footprints, suggesting episodes of subaerial exposure (Petti et al., 2011; Preto et al., 2017). Although lacking direct biostratigraphical markers, this unit is generally assigned to the upper Sinemurian (Boomer et al., 2001; Masetti et al., 2017; Preto et al., 2017).

The Rotzo Formation consists of prevailing grey to dark grey marlstone and bioclastic limestone rich in the peculiar large and aberrant bivalves of the *Lithiotis* Facies. This formation represents deposition in a tropical lagoon, limited seawards by oolitic shoals and bars and landwards by marshes (Bosellini and Broglio Loriga, 1971; Clari, 1975). The formation reaches a maximum thickness of c. 250 m in the depocenter area (Masetti et al., 1998; Posenato and Masetti, 2012) where the studied composite section is exposed. Based on LBF biostratigraphy the formation is considered late Sinemurian to Pliensbachian in age (e.g., Fugagnoli and Loriga Broglio, 1998; Fugagnoli, 2004). The only in situ ammonoid reported in the Rotzo Formation (*Protogrammoceras isseli* trans. *marianii*) occurs within the *Orbitopsella* zone and marks the middle Stokesi Subzone of the lower Margaritatus Zone (basal upper Pliensbachian; Sarti and Ferrari, 1999).

The Misone Limestone is characterized by massive yellowish mudstone and wackestone beds, with chert nodules, foraminifera, radiolarian, sponges, and crinoids. The disappearance of the *Lithiotis* Facies is attributed to the onset of deeper marine conditions. This formation is developed along the western margin of the Trento Platform where it interfingers with shallow- (e.g., Rotzo Formation) or deep-water successions (e.g., Tofino Formation; Castellarin, 1972; Beccarelli-Bauck, 1988; Castellarin et al., 2005). The Misone Limestone is assigned to the Sinemurian–Pliensbachian (Castellarin et al., 2005).

4. Materials and methods

The studied succession was logged at the Malga Zonta (MZ), Monte Toraro (TO; Cimoncello di Toraro, CT), and Monte di Campoluzzo (CL) sections (45°52′03.9″ N 11°14′37.2″ E; 45°52′1.502″ N, 11°16′5.56″ E; 45°52′28.4″ N 11°15′17.8″ E; Fig. 1). Correlation between sections was made by following bedding along the eastern side of Monte Toraro, and the northeastern side of Monte di Campoluzzo (Fig. 1). Although local exposure gaps introduce some uncertainty, the correlation error is estimated not to exceed ±10 m. Hereafter this composite section is referred to as the Toraro–Campoluzzo section (TCs; Fig. 2).

4.1. Taxonomy of LBF and of lithiotid bivalves

All LBF-bearing deposits consists of hard-cemented limestones. The absence of isolated specimens, apart from rare *Orbitopsella* shells, hampered the preparation of oriented sections (i.e., equatorial, axial). Taxonomy of lituolid species (families Everticyclamminidae Septfontaine, 1988; Hauraniidae, Septfontaine, 1988; Lituoliporidae Gušić and Velić, 1978; Loeblich Jr. and Tappan, 1985; Voloshinova, 1958; see Kaminski, 2004) follows the species definitions of Hottinger (1967), Septfontaine (1984, 1985), Fugagnoli and Loriga Broglio (1998), Fugagnoli (1999, 2000), and Fugagnoli and Bassi (2015), whereas the phylogenetic concepts are based on Septfontaine (1988). Shell structures and architectures were distinguished and described following Hottinger (1967, 1978, 2006). Specimens of *Orbitopsella* with shell and protoconch parameters falling close to the limit between two neighbouring species (e.g., Hottinger, 1967; Septfontaine, 1984, 1988; Fugagnoli and Loriga Broglio, 1998; BouDagher-Fadel and Bosence, 2007) were named as *Orbitopsella primaeva/praecursor*. Open nomenclature was used when bad preservation or the absence of suitably

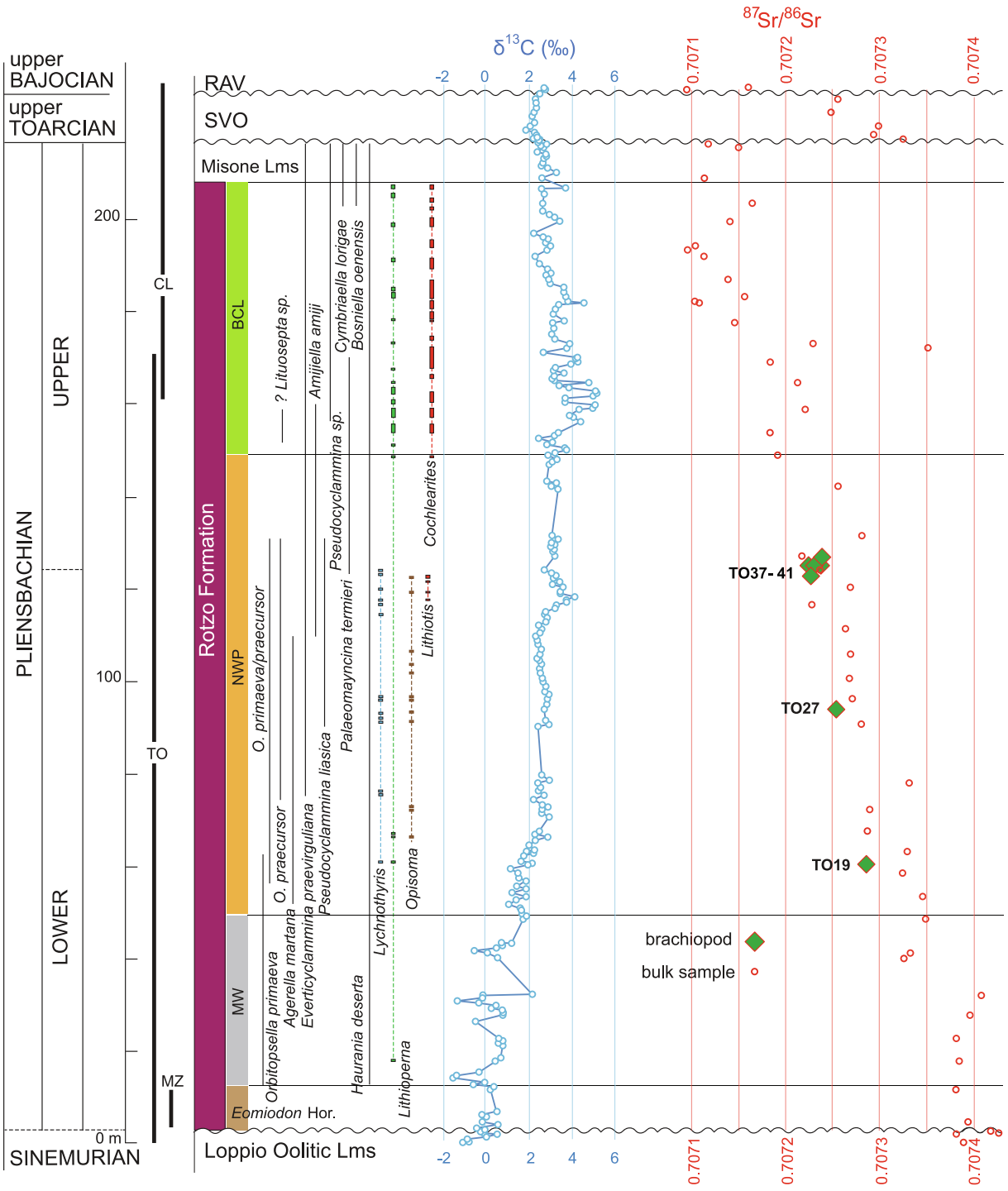

Fig. 2. Chronostratigraphy, lithostratigraphy, lithology, LBF and lithiotid bivalves biostratigraphical distribution, $\delta^{13}C$ and $^{87}Sr/^{86}Sr$ data (see Table S1) of the Toraro–Campoluzzo composite section. The chronostratigraphical age of the lithostratigraphical units and of the biostratigraphical events is taken form the literature (see text for details).
Abbreviations: CL, Monte di Campoluzzo; *Eomiodon* Hor., *Eomiodon* Horizon; Loppio Oolitic Lms, Loppio Oolitic Limestone; Misone Lms, Misone Limestone; MZ, Malga Zonta; SVO, San Vigilio Oolite; RAV, Rosso Ammonitico Veronese; TO, Monte Toraro. (For interpretation of the references to colour in this figure legend, the reader is referred to the web version of this article.)

oriented shell section hindered the observation of diagnostic characteristics.

Isolated bivalve specimens of the *Lithiotis* Facies are rare in the TCs. At outcrop scale their taxonomic identification relied on diagnostic characters observed in oriented sections through the body cavity and umbonal region (Chinzei, 1982; Broglio Loriga and Posenato, 1996; Posenato et al., 2013a, 2013b, 2018, 2022, 2024).

4.2. Geochemical analysis

Powders of bulk rock samples for isotopic analysis were collected in the field, using a battery-operated hammer drill equipped with tungsten carbide bits of diameter ranging from 8 to 14 mm. About 10 to 20 g of powder per sample was produced by drilling a 5–10 cm deep hole after removing the altered surface of the rock. Care was taken to avoid

cement-filled fractures and cavities and recrystallized shell fragments. Samples were collected at an average stratigraphical spacing of c.1 m.

Stable carbon and oxygen isotope compositions were measured on 242 bulk rock carbonate samples using a Thermo Fisher Delta V isotope ratio mass spectrometer coupled to a ThermoQuest Kiel-III (Department of Earth Science, Tohoku University). The samples (c. 0.1 mg) were reacted with 100 % phosphoric acid at c. 72 °C. The isotope ratios are expressed in conventional delta notation (δ ‰) and calibrated to the NBS-19 international standard relative to the Vienna Pee Dee Belemnite (VPDB). External precision (1σ) based on replicate measurements (n = 34) of the laboratory reference material (JCt-1; Okai et al., 2004) was 0.03 ‰ for $\delta^{13}C$ analysis and 0.04 ‰ for $\delta^{18}O$ analyses. All results are given in Table S1.

A subset of 46 bulk rock samples, selected with an average stratigraphical spacing of about 5 m from the 242 samples, was analysed for $^{87}Sr/^{86}Sr$ ratio with a GVI IsoProbe-T thermal ionization mass spectrometer at the Department of Earth and Environmental Sciences, Nagoya University.

Eleven brachiopod shells of *Lychnothyris rotzoana*, from the Rotzo Formation, were examined to assess the quality of preservation. The shell fragments were cut and embedded in epoxy resin. After polishing and etching with 5 % HCl for 10 s, surfaces were coated with gold for imaging with a Scanning Electron Microscope (SEM) Zeiss EVO 40 (University of Ferrara) to check the preservation of the pristine shell fabric. Gold coating was subsequently removed, and thin sections were prepared and analysed with a Nuclide ELM2 cathodoluminescence microscope system operating at 10 kV with a 5–7 mA beam current at the University of Ferrara. Exposure to the electron beam, before taking the photo, was on the order of 15–30 s.

For geochemical analyses, material corresponding to SEM and cathodoluminescence areas was sampled by scratching the cut surfaces, using a microdrill equipped with a 0.3 mm-diameter tungsten carbide drill bit, at the lowest rotation speed. About 1 to 3 mg per sample were collected and analysed for $^{87}Sr/^{86}Sr$ ratio using a Thermo Scientific Neptune MC–ICP-MS at the Centro Interdipartimentale Grandi Strumenti of the University of Modena and Reggio Emilia. A further set of 12 samples, previously analysed for $\delta^{13}C$ and $\delta^{18}O$ isotopes, was also analysed for $^{87}Sr/^{86}Sr$ ratio. All results are given in Table S1. The measured values were adjusted to a value of 0.710248 for NIST SRM 987 (McArthur et al., 2020).

4.3. Strontium isotope stratigraphy

Three horizons of the Rotzo Formation were dated with SIS on well-preserved brachiopod shells: TO19 (one specimen), at 60.4 m, TO27 (two specimens), at 94.4 m, and TO37–41 (five specimens), at 120.4–124.9 m from the base of the section. Numerical ages, chronostratigraphical ages and ammonite zones were determined from the $^{87}Sr/^{86}Sr$ ratios using the LOWESS 6 look-up table of McArthur et al. (2020), which is tied to the Geologic Time Scale of Gradstein et al. (2020). SIS ages derived from the brachiopod shells are given in Table 1. When more than one shell was available from the same stratigraphical level, the mean $^{87}Sr/^{86}Sr$ value was used to calculate the preferred SIS age and the standard error of the mean was combined with the reference curve to define the minimum and maximum age. The five brachiopod shells from levels TO37–41 (120.4–124.9 m from the base of the section) have $^{87}Sr/^{86}Sr$ values within analytical error. They were pooled together because their stratigraphical separation is small and any age difference would be below the SIS resolution.

Of the 58 bulk carbonate samples analysed for $^{87}Sr/^{86}Sr$, 11 were used for SIS, based on assumption that they retained the pristine-seawater isotope ratio signature from which they precipitated or were only minimally altered. The criteria used to select these samples are fully explained in the following section. Numerical ages, chronostratigraphical ages and ammonite zones derived from the bulk rock samples are given in Table 2.

5. Results

5.1. Lithological and stratigraphical patterns

The lowermost part of the TCs (0–2.4 m) corresponds to the Loppio Oolitic Limestone (Fig. 2). Above it, the Rotzo Formation is 205 m thick. The lowermost part, 9.6 m-thick (samples CT8–CT16), corresponds to the *Eomiodon* Horizon, characterized by meter-scale alternations of bioclastic wackestone-packstone with fully marine benthic assemblages and shallow-water black shales containing monospecific or paucispecific bivalve accumulations dominated by *Eomiodon serradensis*, an opportunistic, brackish, shallow-infaunal, veneroid bivalve (e.g., Bassi et al., 2008; Posenato et al., 2013b; Figs. 3 A–B). Because this horizon is partially covered by soil deposits in the Monte Toraro section, additional sampling was conducted along a road exposure in a nearby locality (MZ), located c. 4 km westwards from Monte Toraro (Fig. 1).

Above the *Eomiodon* Horizon, the Rotzo Formation is divided into three informal lithostratigraphical units: mudstone-wackestone (MW), nodular wackestone-packstone (NWP), and biocalcarenites with *Cochlearites–Lithioperna* accumulations (BCL; Fig. 2). The lowermost MW unit is c. 40 m thick and consists of mudstone-wackestone and marlstone alternations (Figs. 1–2) with small-sized bivalve shells, mostly of infaunal species. Bivalves of the *Lithiotis* Facies are represented only by a single bed of *Lithioperna* with small-sized shells (Fig. 2). The middle unit, NWP, is c. 100 m in thickness and is characterized by nodular

Table 1
Strontium Isotope Stratigraphy (SIS) ages derived from the brachiopod shells.

Sample	m from the base	Lithostrat.	$^{87}Sr/^{86}Sr$ corrected[1]	$^{87}Sr/^{86}Sr$ mean	2 s.e. ($\times10^{-6}$)	numerical age (Ma)[2,3]			Chronostrat.[3]	Ammonite zone[3]
						min	preferred	max		
TO19-BR3	60.4	Rotzo Fm NWP	0.707284		12	189.8	190.12	190.6	Pliensbachian	Ibex
TO27–2	94.4	Rotzo Fm NWP	0.707255	0.707253	8	189.2	189.49	189.7	Pliensbachian	Ibex
TO27–2i	94.4		0.707250							
TO37–1-ter	120.4	Rotzo Fm NWP	0.707221	0.707222	2	188.5	188.67	188.9	Pliensbachian	Margaritatus (base)
TO39–1	122.4		0.707222							
TO40(1)-1	122.4		0.707224							
TO40–1 inner	122.4		0.707219							
TO41–3	124.9		0.707224							

[1] The $^{87}Sr/^{86}Sr$ has been corrected for the difference between the value of the standard (NIST SRM 987) measured in the lab and the value used by McArthur et al. (2020) to build the SIS reference curve and look-up table.

[2] The minimum (min) and maximum (max) ages are calculated combining the uncertainty of the samples with the uncertainty of the dataset used to build the reference curve. The uncertainty of the $^{87}Sr/^{86}Sr$ mean value for each stratigraphical level is given as 2 s.e. of the mean when the number of samples (n) is ≥4. When n < 4, the se is calculated from the standard deviation of the mean value of the standards run with the samples (s.d. = 6 × 10^{-6}).

[3] The numerical and chronostratigraphical ages and the ammonite zones corresponding to the $^{87}Sr/^{86}Sr$ values have been taken from the LOWESS 6 look-up table of McArthur et al. (2020), with the exception of the Jamesoni–Ibex zone boundary, which is after Hesselbo et al. (2020).

Table 2
Strontium Isotope Stratigraphy (SIS) ages derived from bulk rock samples.

Sample	m from the base	Lithostrat.	Lithologic interval	$^{87}Sr/^{86}Sr$ corrected [1]	numerical age (Ma) [2, 3]			Chronostrat. [3]	Ammonite zone [3]
					min	preferred	max		
CT11	4.4		*Eomiodon*	0.707392	191.8	192.30	192.8	lower Pliensbachian	Jamesoni
CT15	11.5		MW	0.707381	191.6	192.11	192.6	lower Pliensbachian	Jamesoni
CT39	40		MW	0.707325	191.4	191.08	190.5	lower Pliensbachian	Jamesoni
CT115	116.2		NWP	0.707227	188.2	188.82	189.5	Pliensbachian	Davoei
CT168	126.8		NWP	0.707216	188	188.51	189.3	Pliensbachian	Margaritatus (Stokesi sz)
CT135	148.65	Rotzo Fm	NWP	0.707191	187.5	188.01	188.6	Pliensbachian	Margaritatus (Stokesi sz)
CT143	153.45		BCL	0.707183	187.3	187.86	188.4	upper Pliensbachian	Margaritatus (Subnodosus sz)
CL-56	181.95		BCL	0.707101	182.4	186.16	186.8	upper Pliensbachian	Spinatum (Apyrenum sz)
					182.4	183.11	186.8	lower Toarcian	Falciferum (Exaratum sz)
CL-45	192.95		BCL	0.707094	182.6	185.99	186.6	upper Pliensbachian	Spinatum (Apyrenum sz)
					182.6	183.29	186.6	lower Toarcian	Falciferum (base)
CL-07	222.7	San Vigilio Oolite		0.707247	177	177.87	178.6	upper Toarcian	Variabilis
CL-02	227	RAV		0.707094	168.5	169.01	169.4	upper Bajocian	not available

[1]The $^{87}Sr/^{86}Sr$ was adjusted for the difference between the value of the standard (NIST SRM 987) measured in the lab and the value used by McArthur et al. (2020) to build the SIS reference curve and look-up table.
[2]The minimum (min) and maximum (max) ages are calculated combining the uncertainty of the samples with the uncertainty of the dataset used to build the reference curve. The uncertainty of the $^{87}Sr/^{86}Sr$ value for each sample is given as 2 s.e. and is calculated from the s.d. of the mean value of the standards run with the samples for $n = 1$ (s.d. $= 11 \times 10^{-6}$; 2 s.e. $= 23 \times 10^{-6}$).
[3]The numerical and chronostratigraphical ages and the ammonite zones corresponding to the $^{87}Sr/^{86}Sr$ values have been taken from the LOWESS 6 look-up table of McArthur et al. (2020), with the exception of the Jamesoni–Ibex zone boundary, which is after Hesselbo et al. (2020). The $^{87}Sr/^{86}Sr$ values of samples CL56 and CL45 give two alternative numerical ages because they fall close to the Pliensbachian–Toarcian boundary minimum of the reference curve for marine $^{87}Sr/^{86}Sr$. The ages given in the grey shaded cells are not compatible with the available stratigraphical constraints.
Abbreviations: Fm, Formation; Lms, limestone; RAV; Rosso Ammonitico Veronese; sz, subzone.

wackestone-packstone and marlstone alternations (Fig. 2). This unit contains more diversified benthic assemblages with fully marine taxa such as the alatoform-chambered bivalve *Opisoma excavatum* (Posenato et al., 2013a; Fig. 3C–D) and the terebratulide *Lychnothyris rotzoana* (Bassi et al., 2024; Fig. 4B, D, F). More frequent and larger in size, lithiotids are represented by *Lithioperna* and, in the upper part of the unit, by *Lithiotis* (Fig. 4B–C). The upper unit, BCL, c. 60 m in thickness (Figs. 1–2), consists of thick biocalcarenite beds with metre-thick bivalve mounds of *Cochlearites* (Fig. 5A, C, E–F) and *Lithioperna* (Fig. 5D) with very large shells, more than 30–40 cm in height.

On the eastern flank of Cimoncello di Toraro (CT) and Monte Toraro (Fig. 1), only the lower part of BCL unit is recorded. At 1.870 m altitude (c. 182 m above the base of the succession and 25 m above the base of the BCL unit; Fig. 2), a peculiar 4 m-thick interval characterized by large *Lithioperna* with unusual coarse and thick prismatic shells occurs. This interval was used to correlate the succession with Monte di Campoluzzo (CL, located at c. 2 km north-west; Figs. 1, 5D), where the BCL unit is characterized by frequent *Cochlearites* and *Lithioperna* mounds up to 3 m in thickness and several hundred metres wide. Similar large mounds are also present at the top of the Monte Toraro, above the interval marker (Fig. 5).

At the Monte di Campoluzzo section (Fig. 1), the uppermost Rotzo Formation passes gradually upward into white or yellow mudstone-wackestone, characterized by the occurrence of abundant sponges and crinoids. Lithiotid bivalves disappear at c. 9.6 m below the unconformity marking the base of the San Vigilio Oolite (SVO; Fig. 2). Based on fossil content and rock colour, the bivalve-barren interval is assigned to the Misone Limestone, although typical chert nodules (Castellarin et al., 2005) are locally absent.

The Misone Limestone is overlain by the San Vigilio Oolite (upper Toarcian–lower Aalenian; Clari and Pavia, 2002; Castellarin et al., 2005), which at the Monte di Campoluzzo section consists of 10.4 m of white, yellow or red oolite and oncoid grainstone with frequent cross-bedding structures. The lower and upper limits of the San Vigilio Oolite are sharp and erosional, corresponding to time gaps of various duration (e.g., Masetti et al., 2012).

The last lithostratigraphical unit of the sampled succession is the lower member of the Rosso Ammonitico Veronese (upper Bajocian–middle Callovian; Martire, 1992, 1996; Clari et al., 1984; Martire et al., 2006; Barbieri and Grandesso, 2007), characterized by red nodular pelagic limestone with hardground surfaces and stromatolite

Fig. 3. *Eomiodon* Horizon from the Malga Zonta outcrop and nodular W/P and marl alternation unit of the middle Rotzo Formation, Monte Toraro outcrop. A, *Eomiodon* Horizon of the lower Rotzo Formation (MZ). B, bivalve pavement with *Eomiodon serradensis* and plant remains (MZ). C–D, articulated and fragmented shells of *Opisoma excavatum*, sample CT101.

structures. Only the lowermost part of the Rosso Ammonitico Veronese was sampled at the Monte di Campoluzzo section (Figs. 2, 5G).

5.2. Larger benthic foraminiferal biostratigraphy

The LBF assemblages from the TCs are highly diverse and consist of taxa typical of the Lower Jurassic western Tethys (e.g., Hottinger, 1967; Septfontaine, 1984; Bassoullet, 1997; Fugagnoli, 2004; BouDagher-Fadel and Bosence, 2007; Fugagnoli and Bassi, 2015; Gale and Kelemen, 2017; Sevillano et al., 2020). They include twelve species belonging to ten genera (Fig. 6): *Agerella martana*, *Amijiella amiji*, *Bosniella oenensis*, *Cymbriaella lorigae*, *Everticyclammina praevirguliana*, *Haurania deserta*,? *Lituosepta* sp., *Orbitopsella praecursor*, *Orbitopsella primaeva*, *Paleomayncina termieri*, *Pseudocyclammina liasica*, *Pseudocyclammina* sp.

The FO of *Orbitopsella primaeva* is just above the *Eomiodion* Horizon, at 12 m from the base of the section (Fig. 2). The FO of *Orbitopsella primaeva/praecursor* transitional forms is recorded at 57 m, in the lowermost part of the NWP unit (Fig. 2). These forms co-occur with typical *O. primaeval*, up to 62 m from the base of the section, and with *O. praecursor*, whose FO is at 73 m from the base of the section. The LO of the genus *Orbitopsella* is at c. 130 m, in the upper part of the NWP unit (Fig. 2). *Everticyclammina praevirguliana* appears together with *O. praecursor* and reaches the top of the section. *Agerella martana* occurs between c. 50 m and c. 110 m. *Pseudocyclammina liasica* ranges from 90 m to c. 130 m, disappearing together with *Orbitopsella* spp. *Palaeomayncina termieri* is present from 123 m to 170 m.?*Lituosepta* sp. is recorded in a few beds at c. 150–160 m. *Pseudocyclammina* sp. ranges from 155 m (FO) to the top of the section (i.e., Misone Limestone). *Amijiella amiji* appears at 110 m and disappears at c. 160 m. The Misone Limestone, is characterized by *Cymbriaella lorigae* and *Bosniella oenensis*, along with *Pseudocyclammina* sp., *E. praevirguliana*, and *Haurania deserta*.

The dasycladalean alga *Palaeodasycladus mediterraneus* occurs throughout the Rotzo Formation and is associated with the microfossil *Thaumatoporella parvovesiculifera*. Both these taxa are characteristic of Lower Jurassic inner-platform settings of the western Tethys (e.g., Sartoni and Crescenti, 1959;Chiocchini and Mancinelli, 1978; Chiocchini et al., 1979, 1994; Flügel, 1983; BouDagher-Fadel et al., 2001; Sokač, 2001; Mancinelli et al., 2005).

5.3. Carbon isotope stratigraphy

In the Monte Toraro section, the uppermost 240 cm of the Loppio Oolitic Limestone (Fig. 2) shows $\delta^{13}C$ values ranging between −1.09 ‰ and +0.53 ‰, with the lowest value in bed CT1.

The *Eomiodon* Horizon exposed in the Monte Toraro succession (samples CT8–CT16; Fig. 2) records $\delta^{13}C$ values from −0.07 ‰ at the base to +0.37 ‰ at the top of the interval (Table S1), with minor fluctuations around 0 ‰ in the lower part and a plateau of +0.2 ‰ to +0.5 ‰ in the upper part. In the MZ section (Fig. 3A) the $\delta^{13}C$ profile of the upper 3 m of the *Eomiodon* Horizon shows a plateau with values between +0.88 ‰ and +0.13 ‰ (Table S1), followed by a negative shift to −1.06 ‰ at 3.30 m from the base.

The informal MW unit (samples CT17 to CT47) is characterized by $\delta^{13}C$ values ranging between −1.54 ‰ and +2.19 ‰ (Table S1). The $\delta^{13}C$ profile (Fig. 2) shows an overall rising trend with superimposed high amplitude fluctuations resulting into four negative peaks at 14 m (−1.54 ‰), 26.1 m (−0.48 ‰), 30.6 m (−1.34 ‰), and 41.5 m (−0.53 ‰) (Fig. 2).

The lowermost part of the informal NWP unit (samples CT48–CT63) records $\delta^{13}C$ values from +1.10 ‰ to +2.17 ‰, showing minor fluctuations of less than 0.5 ‰ between adjacent samples and no definite trend (Fig. 2, Table S1). The subsequent interval (samples CT62–CT73; Table S1), displays a rising trend from +1.81 ‰ to +2.99 ‰ (Fig. 2, Table S1), reaching the maximum value at 70.4 m from the base of the section.

This is followed by a c. 38 m thick interval of rather stable $\delta^{13}C$ values, ranging from +2.27 ‰ to +2.99 ‰ (samples CT74 to CT106, from 71.2 to 109.4 m; Fig. 2, Table S1). A distinct positive excursion occurs above, starting at +2.47 ‰ (110.2 m, sample CT107), peaking at +4.2 ‰ (118.05 m, sample CT118) and decreasing to +2.77 ‰ at 123.8 m (sample CT127; Fig. 2, Table S1).

The uppermost NWP unit (samples CT168–CT135, 126.8–148.65 m) shows rather invariant $\delta^{13}C$ values, ranging from +2.88 ‰ to +3.46 ‰ (Fig. 2, Table S1). The lower part of the BCL unit (samples CT136–CL64, 149.15–174.75 m) features a broad positive excursion with superimposed high amplitude fluctuations, reaching peak values of >5 ‰ at around 160 m from the base of the section. The upper BCL unit (CL63–CL32, 175.95–206.75 m) shows $\delta^{13}C$ values of +2.26 ‰ to+4.64 ‰ (Table S1), with an overall decreasing trend and four superimposed

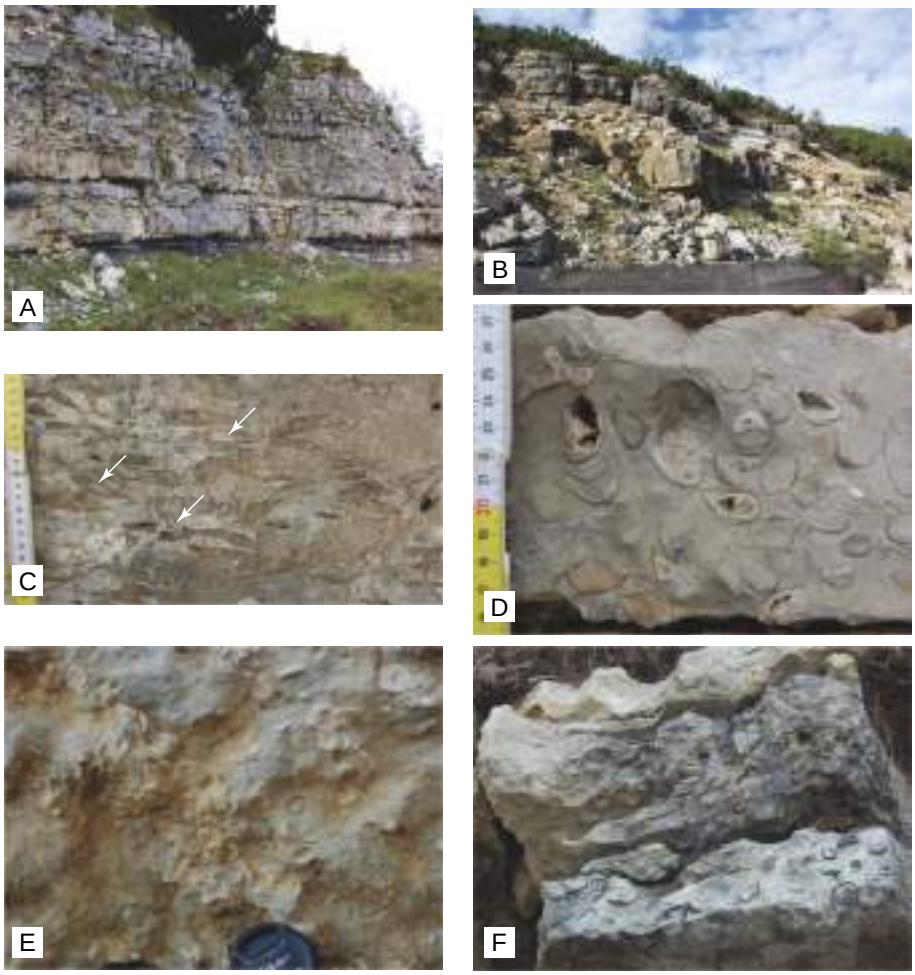

Fig. 4. Details of the nodular W/P and marl alternation unit of the middle Rotzo Formation, Monte Toraro. A, Valico di Valbona; the beds figured in this photograph encompass the bulk samples CT46–CT72 and the brachiopod bed of sample TO27. B, beds with *Lithiotis problematica* and uppermost brachiopod beds with *Lychnothyris rotzoana* (TO39–TO41). C, *Lithiotis problematica* accumulation with transversally sectioned shells; the arrows indicate the umbonal cavity, a peculiar taxonomical character of this species (CT123, TO39). D, F, *Lychnothyris rotzoana* accumulations, bed TO41. E, *Orbitopsella* bed (CT118).

positive excursions (Fig. 2).

The Misone Limestone (samples CL31–CL19) displays a relatively flat $\delta^{13}C$ profile between +2.42 ‰ and+3.36 ‰ (Table S1), with a minor positive fluctuation at the base of the unit (positive peak of +3.36 ‰ at 209.75 m; Fig. 2). In the SVO (samples CL18–CL03) $\delta^{13}C$ values range from +1.90 ‰ to +2.55 ‰ (Table S1) with a low amplitude negative excursion reaching a minimum of+1.90 ‰ at 218.9 m (Fig. 2). In the thin interval of the RAV at the top of the studied section two samples shows $\delta^{13}C$ values of +2.85 ‰ and +2.77 ‰ (Table S1).

5.4. Strontium isotope ratios

The four bulk rock samples of the Loppio Oolitic Limestone have $^{87}Sr/^{86}Sr$ values ranging from 0.707381 to 0.707447 (Table S1), with a scatter of up to 60×10^{-6} over a stratigraphical distance of about 30 cm. The two samples of the *Eomiodon* Horizon in the CTs show values 0.707392 and 0.707381. One sample from the same stratigraphical interval in the MZ section shows a value of 0.707392 (Table S1). The seven bulk rock samples from the informal MW unit exhibits values from 0.707325 to 0.707417 (Table S1) with no consistent stratigraphical trend. In the NWP unit the $^{87}Sr/^{86}Sr$ values of the seven brachiopod shells range from a maximum of 0.707284 for sample TO19 to a minimum of 0.707219 for sample TO40, showing a trend of decreasing values with stratigraphical height (Fig. 2). The bulk rock samples range from a maximum $^{87}Sr/^{86}Sr$ value of 0.707345 at the base of the unit (sample CT53) to a minimum of 0.707191 at the top (sample CT135) (Table S1). These values are more scattered compared to those of the brachiopod shells, with some outliers interrupting the overall decreasing trend. Bulk rock samples show values up to 60×10^{-6} higher than brachiopod shells from adjoining stratigraphical levels (for instance, see bulk samples CT67 and CT60 and the brachiopod shell TO19-BR3; Table S1). The seventeen bulk rock samples from the informal BCL unit range between 0.707094 and 0.707352 (Table S1), displaying a rather wide scatter (Fig. 2). Three samples in the Misone Limestone have $^{87}Sr/^{86}Sr$ values ranging from 0.707113 to 0.707148. The five bulk rock samples from the SVO range from a maximum of 0.707327 at the base of the unit to a minimum of 0.707247 close to the top. Finally, two samples at the base of the RAV have values of 0.707094 and 0.707159.

6. Discussion

6.1. Assessing the preservation of the marine strontium isotope ratio in brachiopod shells and bulk rock samples

Eleven brachiopod shells collected from the Rotzo Formation were examined with SEM and cathodoluminescence to assess their state of preservation. Specimens were considered well-preserved when (1) they retained original microstructural features observable under the SEM, and (2) the corresponding portion of the thin sections were non-luminescent under cathodoluminescence (e.g., Garbelli et al., 2012).

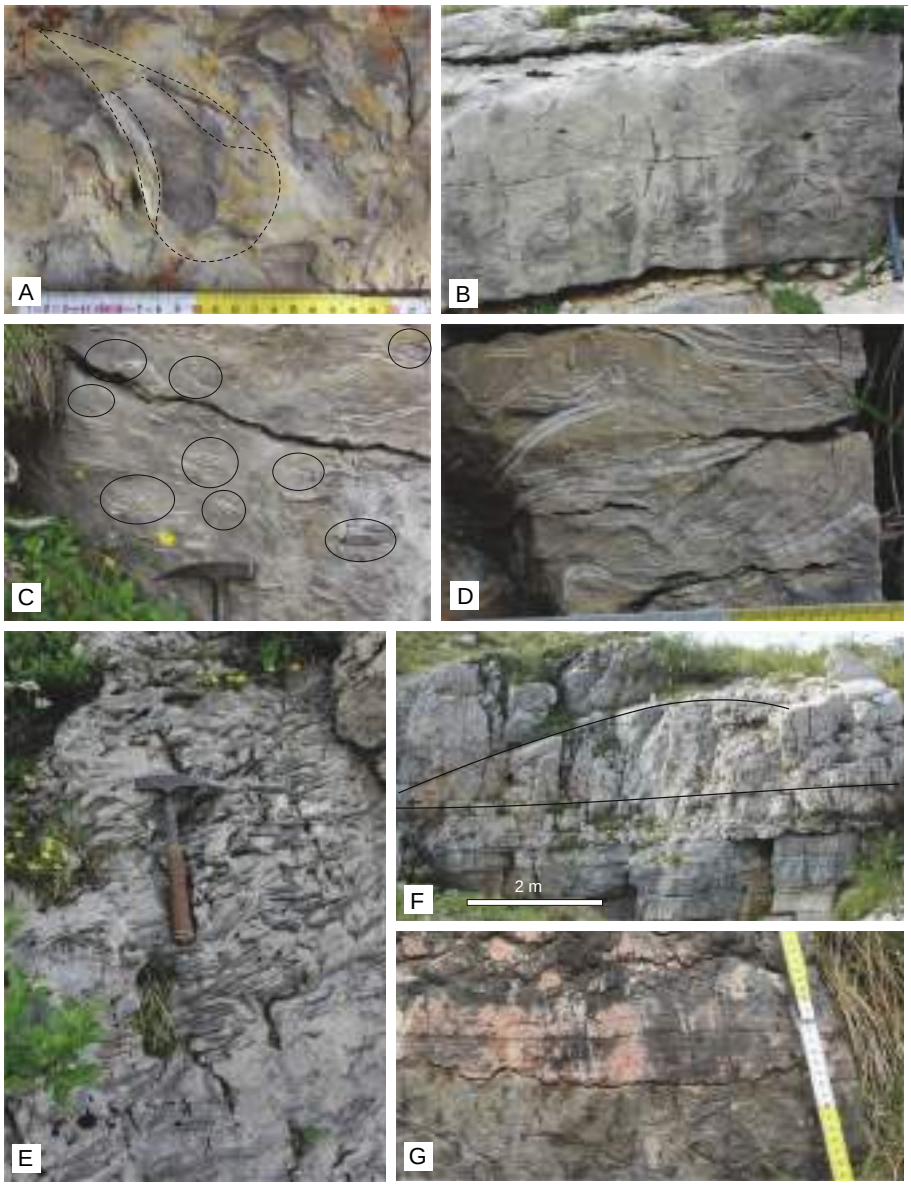

Fig. 5. Details of the biocalcarenites with *Cochlearites–Lithiperna* accumulations unit of the upper Rotzo Formation, Monte Toraro (CT, TO) and Campoluzzo (CL). A–F, biocalcarenite beds with metre-thick bivalve mounds of *Cochlearites* and *Lithioperna* (CT, TO, CL). A, bed surface with a *Cochlearites loppianus* valve laying with the inner surface upwards, CT150. B–C, *Cochlearites* and *Lithioperna* bed, the circled shells show the taxonomical characters for the identification of *Cochlearites*, CT153. D, articulated *Lithioperna scutata* shells, CL67. E, flank of a *Cochlearites loppianus* mound, upper part of the Toraro succession. F, *Cochlearites* mound, CT165–CT167. G, unconformable and erosional contact between the San Vigilio Oolite and the Rosso Ammonitico Veronese, CL01–CL02.

This combined approach allowed us to evaluate both the structural integrity and the reliability of the geochemical data prior to their use in SIS.

The seven brachiopod shells ultimately selected for SIS (Table 1) show good preservation of both the fibrous and columnar layer microstructures (Fig. 7). In these specimens, the fibres display a well-defined outline and the columns of the tertiary shell layer show micrometric banding of suggesting minimal diagenetic alteration. Conversely, samples with disrupted microstructure with evidence of dissolution were excluded, as these features are indicative of diagenetic modification and loss of primary isotopic information. Luminescence, controlled primarily by the molar ratio of Fe/Mn, serves a good proxy for diagenesis, given that pristine marine carbonate is typically depleted in Fe and Mn (Machel, 2000). Accordingly, non-luminescent shells are interpreted as least affected by secondary alteration, whereas luminescent portions reflect Mn enrichment, usually derived from the breakdown of organic matter during diagenesis (Fujioka et al., 2025). In line with the diagenetic experiments of Fujioka et al. (2025), our observations indicate that Mn-enriched, luminescent domains correspond to shell portions where original carbon and oxygen isotope compositions have been overprinted. Such domains are therefore unsuitable for paleoenvironmental reconstructions or stratigraphical purposes. By combining SEM-based microstructural screening with cathodoluminescence imaging we were able to identify brachiopod shells most likely to preserve primary isotopic signatures, thus maximizing the reliability of SIS results. The analysed shell fragments are non-luminescent across most of their structure, except for portions along fractures permeated by late diagenetic fluid or zones with disrupted microstructure. The fibrous layer shows poor to weak luminescence, while the columnar layer is consistently the darkest part of the shell (Fig. 8). The surrounding rock matrix is similarly poorly to slightly luminescent, comparable to the fibrous layer, except in areas hosting cements precipitated by late diagenetic fluids.

By contrast, bulk rock carbonate samples represent mixtures of

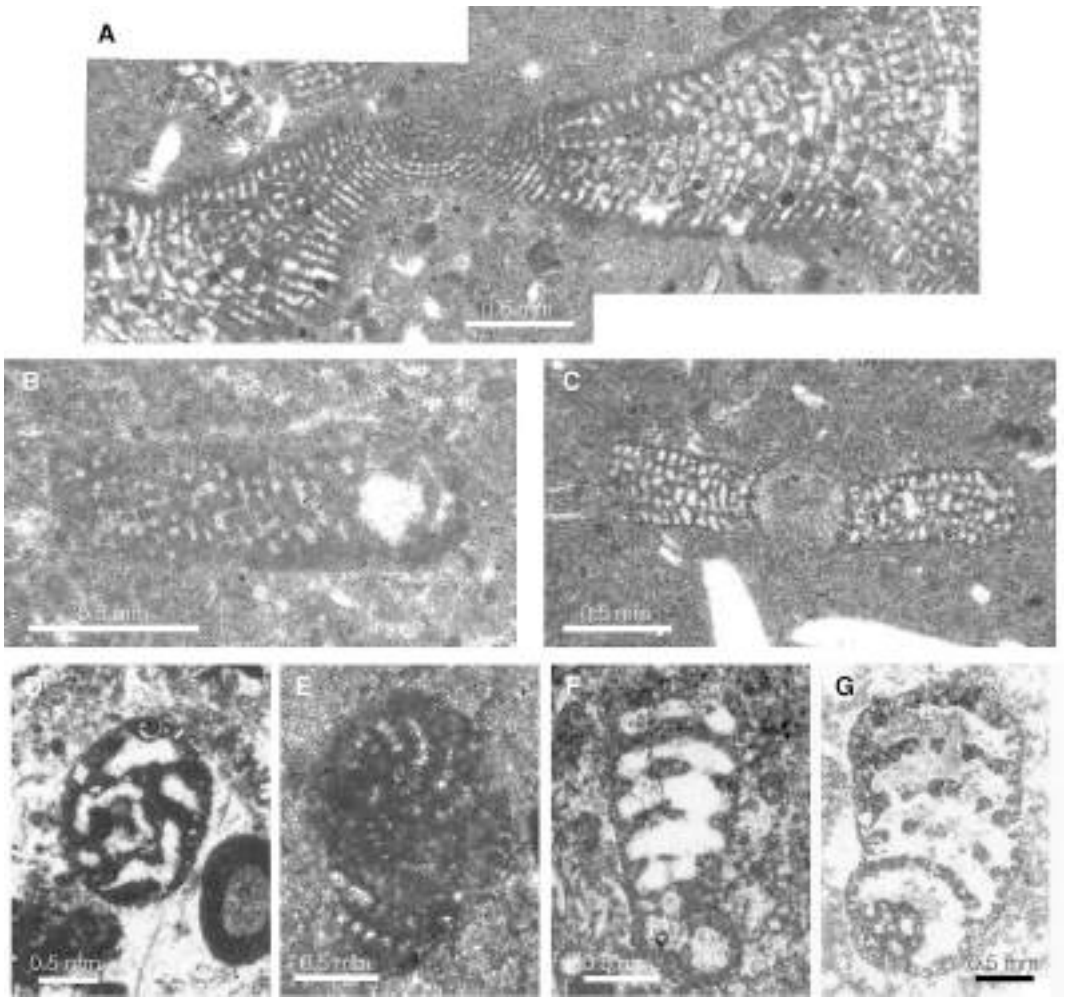

Fig. 6. Selected LBF lituolid species from the Monte Toraro (TO) and Monte di Campoluzzo (CL) sections, Rotzo Formation. A, *Orbitopsella primaeva*; B-form, TO. B, *Orbitopsella primaeva*; A-form, TO. C, *Orbitopsella praecursor*; A-form, TO. D, *Everticyclammina praevirguliana*; A-form, TO. E, *Pseudocyclammina liasica*; A-form, TO. F, *Bosniella oenensis*; A-form, CL. G, *Cymbriaella lorigae*; A-form, CL.

pristine marine precipitates and diagenetic material introduced through interaction with marine and non-marine fluids. Their geochemical composition is, therefore, commonly altered to some degree, causing their strontium isotopic ratio to deviate from contemporaneous seawater values (e.g., Banner, 1995; Swart, 2015). The high-amplitude fluctuations and large scatter (up to 50–150 $\times$ 10^{-6} over stratigraphical intervals of <10 m) observed in the $^{87}Sr/^{86}Sr$ values ratios of most bulk rock samples (Fig. 2, Table S1) clearly indicate diagenetic overprinting or contamination by non-marine strontium. Such variability is incompatible with the expected smooth evolution of marine $^{87}Sr/^{86}Sr$ over time, a consequence of the long residence time of strontium in the seawater (McArthur, 1994; McArthur et al., 2016, 2020).

The following criteria were applied to select a subset of bulk rock samples for SIS, under the assumption that they retained the pristine isotope ratio of the seawater or were only minimally altered. We started by comparing the $^{87}Sr/^{86}Sr$ values of bulk rock samples and well-preserved brachiopod shells from adjoining levels (within <4 m; Table S1). Most bulk rock samples have $^{87}Sr/^{86}Sr$ values that are offset toward higher values relative to the well-preserved brachiopods (Fig. 2). This offset supports the hypothesis that diagenetic alteration or contamination with strontium of continental origin moved the pristine marine values of carbonates precipitated from seawater toward more radiogenic values, a well-known pattern commonly reported in the scientific literature (e.g., Veizer and Compston, 1974; McArthur, 1994; Banner, 1995; Brand et al., 2011; Frijia et al., 2015; Yamamoto et al., 2017; Table S1).

Two bulk samples with $^{87}Sr/^{86}Sr$ values within analytical error of well-preserved brachiopods from adjoining stratigraphical levels were considered non-altered, or minimally affected by diagenesis and/or contamination, and they were retained or SIS (CT168 and CT115; Fig. 9, Table S1). Under the hypothesis that in the studied succession diagenetic alteration moved the original $^{87}Sr/^{86}Sr$ ratios toward higher values, in intervals lacking brachiopod shells, we retained for SIS the bulk rock samples showing the lowest $^{87}Sr/^{86}Sr$ values (Fig. 9). Two samples complying with this criterion were discarded because their Sr isotope ratio would produce a SIS age older than a sample stratigraphically below. This is the case of sample CT5, in the Loppio Oolitic Limestone, and of sample CL31, in the Misone Limestone (Fig. 9, Table S1). The plot of $^{87}Sr/^{86}Sr$ vs the stratigraphical position (metres from the base of the section; Fig. 9), shows that segments connecting the subset of samples selected for SIS (bulk rock samples with lowest $^{87}Sr/^{86}Sr$ values and well-preserved brachiopod shells) display only minor changes in inclination (Fig. 9). Assuming a nearly constant long-term accumulation rate and the absence of significant gaps, this pattern aligns with the accepted view of linear changes in marine $^{87}Sr/^{86}Sr$ ratio through geological time (McArthur et al., 2016), supporting the hypothesis that the selected bulk rock samples preserved their pristine marine strontium isotope ratio or were only minimally altered.

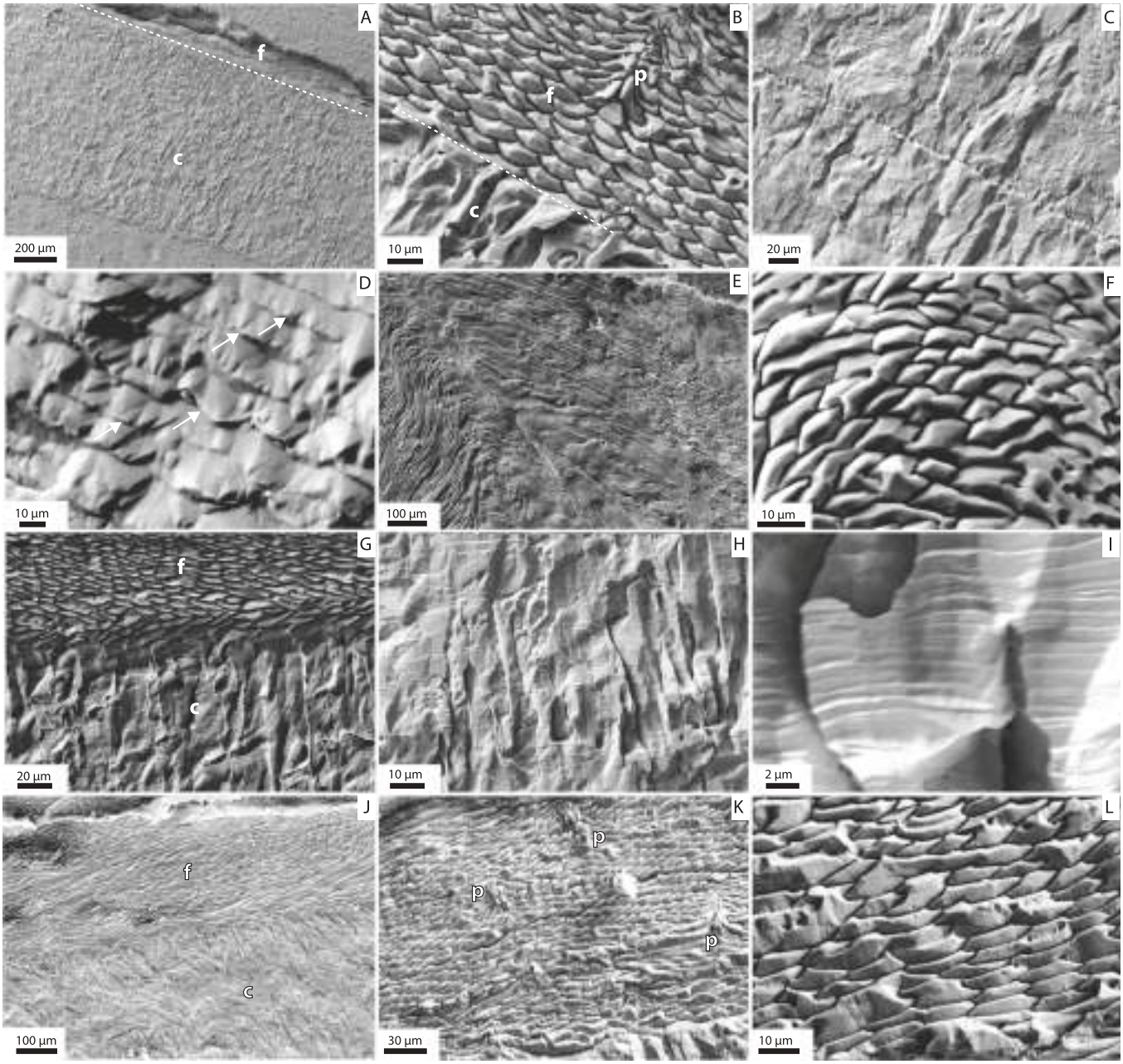

Fig. 7. Shell microstructure of brachiopods specimens observed with the scanning electron microscope. A, shell sequence composed of an outer fibrous (f) and inner columnar (c) layer, specimen TO19-BR3. B, detail of A showing the fibres (f), with a keel and saddle outline crossed by a punctum (p), and the boundary with the columns (c). C, columnar layer of specimen TO19-BR3. D, detail of C s showing accretionary bands (arrows) in a column. E, fibres of the umbonal region, specimen TO27–2. F, details of D showing morphologically preserved fibres with keel and saddle outline. G, shell sequence of the middle shell region with fibres (f) and columns (c). H, columnar layer of the specimen TO37–1-ter. I, detail of H with accretionary bands. J, shell sequence composed of an outer fibrous (f) and inner columnar (c) layer, specimen TO40–1 (inner). K, fibrous layer (f) crossed by small punctae (p), specimen TO41–3. L, detail of M showing the fibres with keel and saddle outline. The outermost shell surface is at the top of the images.

6.2. *Strontium isotope stratigraphy of the Rotzo Formation*

SIS ages of the selected brachiopod shells and bulk rock samples were used to assign numerical ages, chronostratigraphical positions and corresponding ammonite zone to lithostratigraphical intervals recognized in the studied TCs (Fig. 9, Tables 1–2).

Sample CT11 in the *Eomiodon* Horizon yielded a SIS age of 192.30 Ma, corresponding to the lower Pliensbachian Jamesoni Zone (Fig. 9, Table 2). This confirms the Pliensbachian age inferred by previous Authors (Posenato and Masetti, 2012; Posenato et al., 2013b). Notably, sample CT11 and sample MZ9 from the *Eomiodon* Horizon of the MZ section show the same $^{87}Sr/^{86}Sr$ ratio (Table S1).

Sample CT15, at the base of the MW unit, gives a SIS age of 192.10 Ma and sample CT39, at 40 m from the base of the TCs, provides a SIS age of 191.08 Ma (Table 2). These two samples constrain the lower Pliensbachian age of the MW unit and support a correlation with the Jamesoni Zone.

The brachiopod shell of sample TO19, at 60.4 m from the base of the section, in the lower part of the NWP unit, yields a SIS age of 190.12 Ma, which corresponds to the lower Pliensbachian (Fig. 9, Table 1). The two brachiopod shells of sample TO27 provide a SIS age of 189.49 Ma, which is located within the Ibex Zone, based on the calibration of Hesselbo

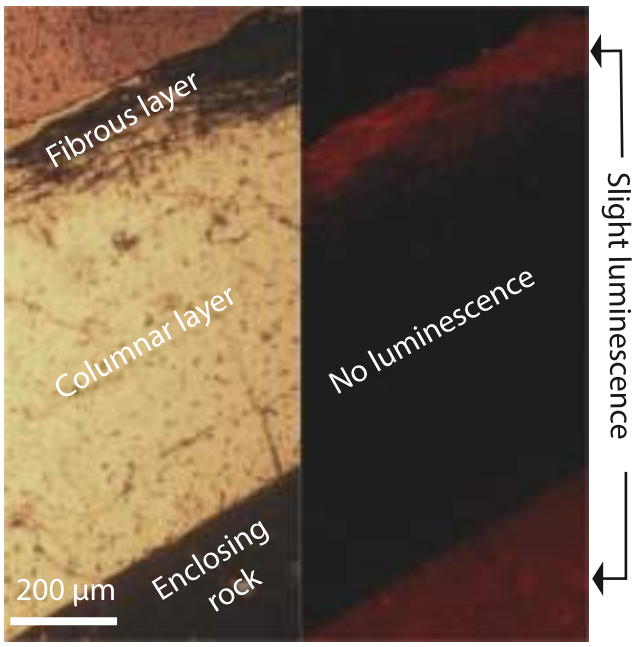

Fig. 8. Luminescence features of the brachiopod specimen TO19-BR3. The image captured with the cathodoluminescence microscope system (right) is coupled with optical photomicrographs under transmitted light (left). The outermost shell surface is at the top of the image.

et al. (2020) (Table 1).

Sample CT115, at 116.2 m from the base of the section, yields a SIS age of 188.82 Ma. This age is congruent to the upper Pliensbachian Davoei Zone. The brachiopod shells of samples TO37–TO41 give a SIS age of 188.67 Ma, which corresponds to the boundary between the Davoei and the Margaritatus zones (McArthur et al., 2020; Fig. 9, Table 1).

Sample CT168, at 126.8 m from the base of the section, gives a SIS age of 188.50 Ma, corresponding to the lowermost part of the upper Pliensbachian lower Margaritatus Zone (Stokesi Subzone) according to the direct calibration in the look-up table of McArthur et al. (2020) (Table 2 and Fig. 9). Sample CT135, at the top of the NWP unit (at 148.65 m from the base of the section) gives a SIS age of 188.01 Ma, corresponding to the Margaritatus Zone (uppermost part of the Stokesi Subzone; Table 2).

Sample CT143, in the lowermost part of the BCL unit, at 153.45 m from the base of the section, gives a SIS age of 187.86 Ma, corresponding to the upper Pliensbachian Margaritatus Zone (Subnodosus Subzone). Sample CL56, at 177.15 m from the base of the section, gives a SIS age of 186.16 Ma, which falls within the Spinatum Zone according to the calibration of McArthur et al. (2020) (Fig. 9, Table 2). Sample CL45, in the upper part of the BCL unit (at 192.95 m from the base of the TCs), gives a SIS age of 185.99 Ma, in the upper Pliensbachian Spinatum Zone (Table 2). As stated above, we hypothesize that the $^{87}Sr/^{86}Sr$ ratio of sample CL-31 was shifted toward higher value by digenetic alteration. For this reason, we excluded it from the SIS dataset. Since no evidence of an unconformity is observed at the top of the Rotzo Formation, and considering the age obtained from sample CL45 in the upper part of the BCL unit, we tentatively accept an uppermost Pliensbachian age for the Misone Limestone.

Sample CL07, at 6 m above the base of the San Vigilio Oolite, yielded a SIS age of 177.87 Ma, corresponding to the upper Toarcian (Variabilis Zone). This result is consistent with the age inferred from biostratigraphical constraints for the base of this formation (Callomon et al., 1994).

Sample CL02, at the base of the Rosso Ammonitico Veronese, gives a SIS age of 169.01 Ma, corresponding to the upper Bajocian. This age is in good agreement with that attributed to the lower member of the RAV based on ammonites (Martire, 1996).

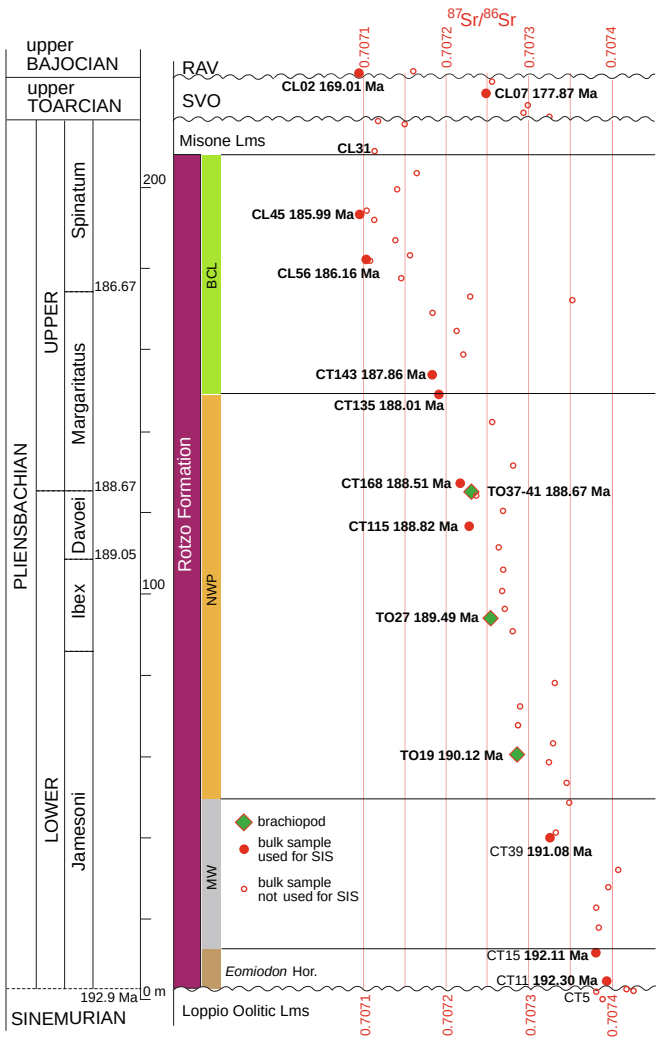

Fig. 9. Strontium isotope stratigraphy of the Toraro–Campoluzzo composite section. The $^{87}Sr/^{86}Sr$ values of well-preserved brachiopod shells and of a subset of the bulk rock samples have been used to assign numerical and chronostratigraphical ages and to correlate to standard ammonite zones. The conversion from Sr isotope ratios to ages is made by using the LOWESS 6 look-up table of McArthur et al. (2020), which is tied to the Geologic Time Scale of Gradstein et al. (2020). The criteria applied to select the bulk samples for strontium isotope stratigraphy are explained in paragraph 6.2. The data of strontium isotope stratigraphy are summarized in Tables 1–2. For abbreviations see Fig. 2.

6.3. *Assessing the reliability of the carbon isotope record of the Toraro–Campoluzzo composite section as a stratigraphical tool for global correlations*

The carbon isotope record of shallow-water carbonates is widely used as a stratigraphical tool for global correlation and chronostratigraphical calibration (e.g., Halverson et al., 2005; Maloof et al., 2005; Huck et al., 2011; Parente et al., 2007). However, several potential pitfalls complicate the correlation between carbon isotope records derived from shallow-water carbonates and those representing the global ocean, as preserved in deep-water sediments (e.g., Immenhauser et al., 2008; Swart, 2008, 2015; Ahm and Husson, 2022, and references therein). These pitfalls can be broadly grouped into three general categories: (1) palaeoceanographic effects, which may decouple the

chemistry of neritic water masses from that of the open ocean (see Immenhauser et al., 2008, for a review); (2) compositional biases, arising from the much greater heterogeneity of shallow-water carbonate sediments when compared with the relatively homogeneous open ocean deep-water carbonate sediments (e.g., Geyman and Maloof, 2021); (3) diagenetic alteration, which for carbon isotopes is mainly driven by syndepositional respiration of organic matter within marine pore waters and by interaction with meteoric water during early diagenesis (e.g., Patterson and Walter, 1994; Allan and Matthews, 1982; Swart, 2015).

In this section, we assess the impact of compositional and diagenetic effects on the stable isotopes record of the studied section by examining crossplots of carbon and oxygen isotope ratios. Nearly all analysed bulk rock samples have $\delta^{18}O$ values within the range of Pliensbachian subtropical shallow seawater, as defined by well-preserved brachiopod shells (Figs. 10, S1; Veizer and Prokoph, 2015). Since the oxygen isotope ratio of carbonates is easily altered during diagenesis, even at low water-to-rock ratios (Banner and Hanson, 1990), this observation suggests that diagenesis did not play a major role in significantly modifying our dataset.

By contrast, carbon isotopes of carbonates are generally more resistant to diagenetic alteration, as they are buffered by the large amount of carbon supplied through carbonate dissolution compared to the relatively minor contribution of carbon from diagenetic fluids (Banner and Hanson, 1990). Nevertheless, deviations from the expected primary seawater signal are evident in the dataset. Many samples fall outside the range of Pliensbachian tropical seawater (Figs. 10, S1), as defined by the compilation of well-preserved belemnite and brachiopod shells in Prokoph et al. (2008). Specifically, most samples from the BCL unit, and nearly half of those from the NWP unit, displays $\delta^{13}C$ values up to 2 ‰ higher than the maximum value recorded by coeval brachiopods and belemnites. A possible explanation is that this subset of samples reflects the original higher aragonite content of their depositional setting, as aragonite tends to yield $\delta^{13}C$ values shifted toward higher values (Romanek et al., 1992). This interpretation is also consistent with the observation that nearly all samples with $\delta^{13}C$ values >3 ‰ (i.e., outside the range of well-preserved Pliensbachian brachiopods and belemnites, whose shells are made of low-Mg calcite) are from levels characterized by accumulations of lithiotid bivalves (Fig. 2), whose thick shells were dominantly aragonitic. Furthermore, apart from these anomalously positive values ($\delta^{13}C$ values >3 ‰), the remaining samples from other lithologic intervals exhibit largely overlapping $\delta^{13}C$ ranges (Figs. 10, S1). This pattern suggests that, outside the influence of aragonite-rich lithiotid accumulations, there is no compelling evidence for a strong facies-related control on the $\delta^{13}C$ signal.

Another potential source of compositional bias lies in the heterogeneity of $\delta^{13}C$ values in the dissolved inorganic carbon ($\delta^{13}C_{DIC}$) of seawater over shallow-water platforms. Local photosynthesis and calcification of marine organisms preferentially remove ^{12}C from the seawater, thereby enriching the residual DIC in ^{13}C (Swart et al., 2009). These processes can generate isotopic fractionations of up to approximately 8 ‰ (Emrich et al., 1970; Romanek et al., 1992). Therefore, when establishing carbon isotope stratigraphy from shallow-water carbonates, it is critical to target settings less affected by strong $\delta^{13}C_{DIC}$ heterogeneity. In the case study, as we analysed carbonates deposited in a lagoonal palaeoecosystem, the effect of $\delta^{13}C_{DIC}$ heterogeneity is likely minimal.

Starting from Allan and Matthews (1982), a positive correlation between $\delta^{13}C$ and $\delta^{18}O$ values has been often invoked as evidence for diagenetic alteration by waters of mixed meteoric-marine origin. In our dataset, the crossplots in Fig. 10 (see also Fig. S1) show that a strong positive correlation ($r^2 = 0.95$) is present only in the samples of the Loppio Oolitic Limestone, at the base of the studied section. This is consistent with the evidence of subaerial exposure at the top of this unit, both in the studied section and in other areas of the Trento Platform (Petti et al., 2011; Preto et al., 2017). By contrast, the Rotzo Formation shows neither sedimentological nor petrographic evidence of subaerial exposure and/or meteoric diagenesis. Moreover, no significant covariance between carbon and oxygen isotope ratios is observed (Figs. 10, S1). Importantly, the $\delta^{18}O$ values largely overlap with those of well-preserved brachiopod shells (Figs. 10, S1; Prokoph et al., 2008; Veizer and Prokoph, 2015). Taken together, these lines of evidence support the interpretation that the carbon isotope record of the Rotzo Formation could preserve, at least in the major features, the primary signal of the global ocean. In the following sections we explore the correlation of this record with reference curves of sections from deep-water settings, using the SIS age constraints as tie points.

6.4. *Comparing the carbon isotope record of the Rotzo Formation with reference $\delta^{13}C$ curves*

Figure 11 shows a correlation panel comparing the carbon isotope profile of the studied section with those of two well-documented

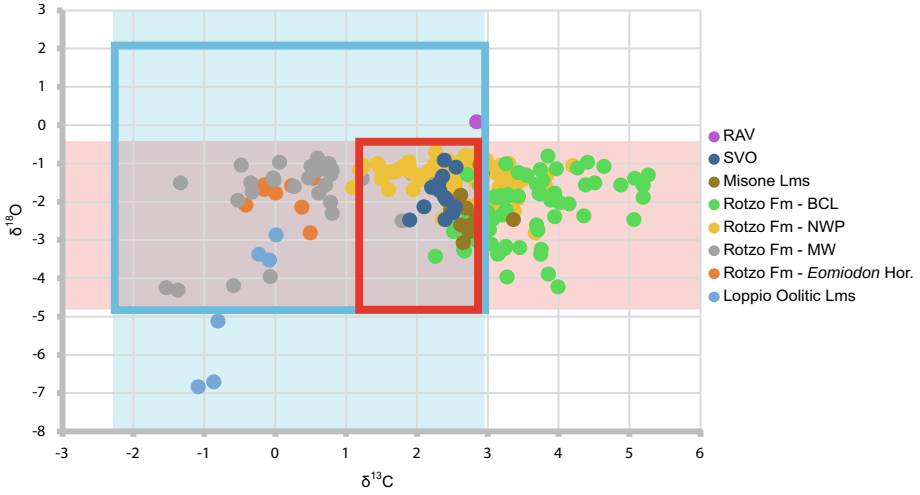

Fig. 10. Crossplot of $\delta^{13}C$ and $\delta^{18}O$ values of bulk rock samples from the Toraro–Campoluzzo composite section (see dataset in Table S1). The shaded red area delimits the region of $\delta^{18}O$ values measured on well-preserved brachiopod shells of Veizer and Prokoph, 2015. The shaded blue area delimits the region of $\delta^{13}C$ values from well-preserved brachiopod and belemnite shells of Prokoph et al., 2008. A strong positive correlation ($r^2 = 0.95$) between $\delta^{13}C$ and $\delta^{18}O$ values is present in samples from the Loppio Oolitic Limestone. For abbreviations, see Fig. 2. (For interpretation of the references to colour in this figure legend, the reader is referred to the web version of this article.)

successions in the UK: Robin Hood's Bay in the Cleveland Basin (Korte and Hesselbo, 2011) and the Mochras Core in the Cardigan Bay Basin (Storm et al., 2020). These two successions are used as reference sections for carbon isotope stratigraphy because they are calibrated against the GTS 2020 by means of standard ammonite zonation and are considered as reliable records of global carbon isotope events. For the Trento Platform, we plotted a smoothed curve obtained by applying a 5-points moving average to the carbon isotope ratios listed in Table S1. For the Cleveland Basin we used the data provided in the supplementary material of Korte and Hesselbo (2011). In particular, the curve labelled "δ^{13}C shells" in Fig. 11 is a 5-points moving average of the carbon isotope ratios from belemnite, brachiopod and bivalve shells with Sr > 400 ppm and Mn < 250 ppm, considered to be well preserved by Korte and Hesselbo (2011). The curve labelled "δ^{13}C wood" is a 5-points moving average of δ^{13}C values from wood samples (Table S1 in Korte and Hesselbo, 2011). For the Mochras core in the Cardigan Bay Basin we plotted a 7-points moving average of the δ^{13}C TOC values reported in the supplementary material of Storm et al. (2020). The two reference sections of Korte and Hesselbo (2011) and Storm et al. (2020) are constrained by a well-established ammonite zonation, whereas the position of the ammonite zone boundaries in the studied section has been inferred on the basis of the SIS data (see paragraph 6.2).

The tentative correlation framework presented in Fig. 11 suggests that the long rising trend of the δ^{13}C curve, extending from the base of the Rotzo Formation to the lower part of the NWP unit corresponds to the rising arm of Sinemurian–Pliensbachian boundary event (SPBE) as delimited in the Mochras core by Storm et al. (2020, fig. 3). The same event has also been recognized in the Cleveland Basin curve of Korte and Hesselbo (2011, fig. 6), and in many other sections of northern and southern Tethyan margins (e.g., Morettini et al., 2002; Schootbrugge van de et al., 2005; Speranza and Parisi, 2007; Woodfine et al., 2008; Marino and Santantonio, 2010; Duarte et al., 2014; Bougeault et al., 2017), including other successions of the Trento Platform (Franceschi et al., 2014, 2019). This correlation supports the attribution of the *Eomiodon* Horizon and of the MW unit of the Rotzo Formation to the lower part of the Jamesoni Zone, as independently inferred from the SIS data (see paragraph 6.2).

Higher up in the section, we propose that the positive δ^{13}C excursion observed in the lower part of the BCL unit of the Rotzo Formation correlates with the late Pliensbachian positive event identified in the δ^{13}C curves of the Cardigan Basin (Fig. 11). A correlative positive excursion, referred to the Subnodosus positive event in Storm et al. (2020, fig. 3), is

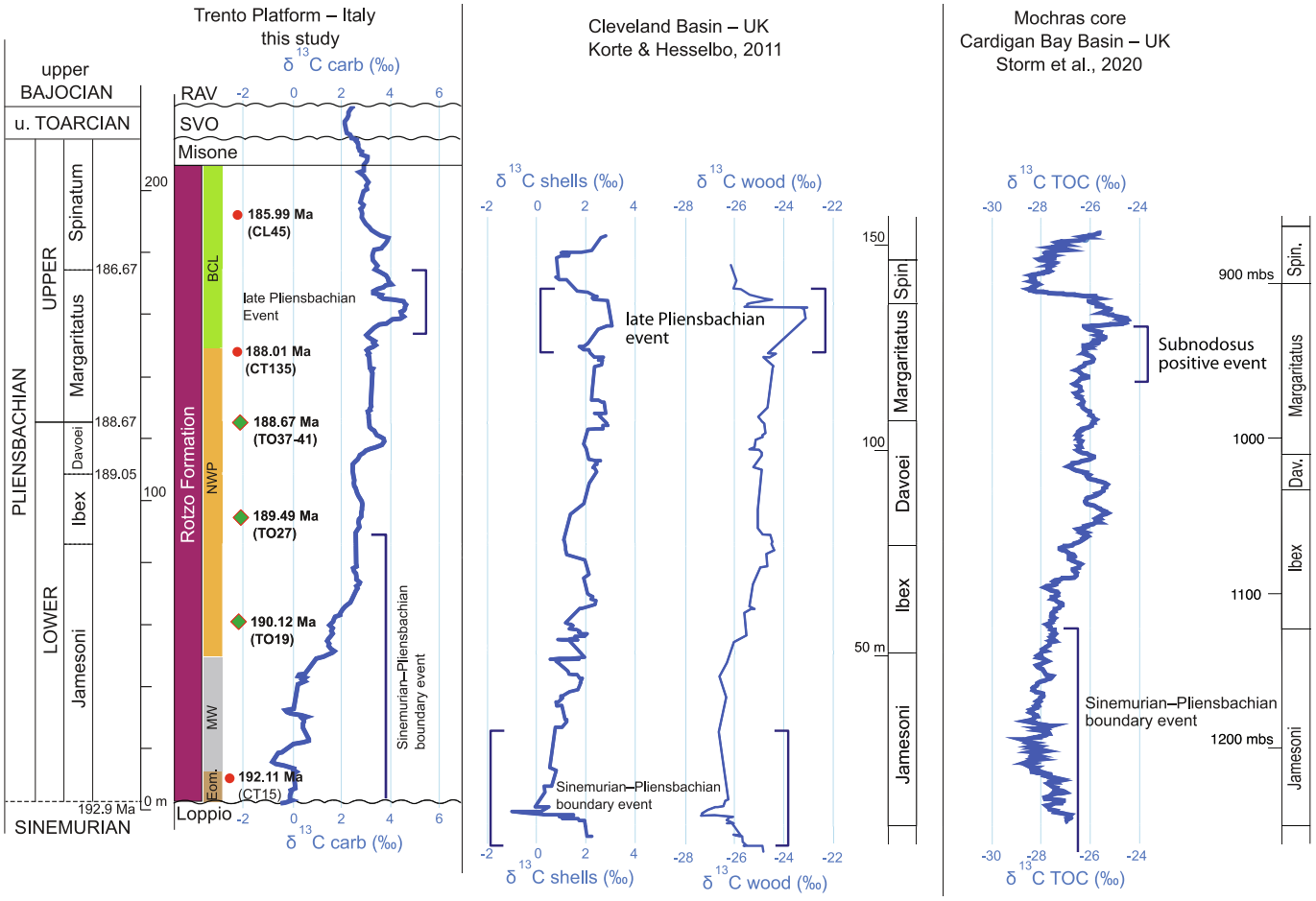

Fig. 11. Carbon isotope stratigraphy of the Toraro–Campoluzzo composite section. The carbon isotope profile of the studied section has been correlated with the profiles of two well-dated reference sections that preserve the record of global carbon isotope vents of the Early Jurassic Ocean: the Robin Hood's bay section in the Cleveland Basin (Korte and Hesselbo, 2011) and the Mochras core in the Cardigan Bay Basin (Storm et al., 2020). The δ^{13}C carb curve for the Trento Platform (this study) has been obtained by applying a 5-points moving average to the δ^{13}C data of the bulk samples of the Toraro-Campoluzzo composite section (the data are listed in Table S1). The δ^{13}C shells curve of the Cleveland Basin is a 5-points moving average of the carbon isotope ratios of well-preserved belemnite, brachiopod and bivalve shells with Sr > 400 ppm and Mn < 250 ppm (data in Table S1 of Korte and Hesselbo, 2011). The curve labelled as "δ^{13}C wood" is a 5-points moving average of the carbon isotope ratios of the wood samples (Korte and Hesselbo, 2011, Table S1). For the Mochras core in the Cardigan Bay Basin we have plotted a 7-points moving average of the δ^{13}C TOC values contained in the supplementary material of Storm et al., 2020. The Sinemurian–Pliensbachian boundary event and the Late Pliensbachian Event are recognized in the carbon isotope profile of the Trento Platform by visual comparison with the reference curves. The correlation of carbon isotope events is aided by the chronostratigraphical framework established by strontium isotope stratigraphy. For abbreviations see Fig. 2.

also evident in the Mochras $\delta^{13}C$ record, although its delimitation differs (Fig. 11). Comparable positive excursions have likewise been documented in other sections from both northern and southern Tethyan margins and in the Paris Basin (e.g., Schootbrugge van de et al., 2010; Peti et al., 2017; Mercuzot et al., 2019; Schöllhorn et al., 2020). This correlation supports assigning the base of the BCL unit of the Rotzo Formation to the upper part of the Margaritatus Zone and placing the Margaritatus–Spinatum zone boundary, both tentatively inferred from the SIS data (Fig. 11).

6.5. *Chronostratigraphical calibration of larger benthic foraminiferal events and lithiotid bivalves*

The age constraints established through the integration of SIS and carbon isotope stratigraphy (paragraphs 6.2 and 6.4) provide the basis for assigning a chronostratigraphical age to the biostratigraphical events of LBF and to the onset and demise of the *Lithiotis* Facies in the Rotzo Formation (Fig. 12).

6.5.1. *Chronostratigraphical distribution of larger benthic foraminifera*

Two LBF intervals can be distinguished in the studied section: the *Orbitopsella* interval and the post-*Orbitopsella* interval. These intervals correspond to those originally described by Fugagnoli and Loriga Broglio (1998) and Fugagnoli (2004) in the Trento Platform. The lower limit of the *Orbitopsella* interval is marked by the FO of *Orbitopsella primaeva*, whereas its upper limit is marked by the LO of the genus *Orbitopsella* and of *Pseudocyclammina liasica*. In the Monte Toraro section, the FO of *Orbitopsella primaeva* is just above the *Eomiodon* Horizon, at the base of the MW unit of the Rotzo Formation. In other areas of the Trento Platform the FO of *Orbitopsella primaeva*, in association with *Lituosepta recoarensis*, is located in the *Eomiodon* Horizon (Val Gola section in Fugagnoli, 1998).

Based on the SIS age of samples CT15, and on the additional constraint offered by the recognition of the Sinemurian–Pliensbachian Boundary Event in the $\delta^{13}C$ curve of the TCs, the FO of *O. primaeva* in the Rotzo Formation can be assigned to the lowermost Pliensbachian, correlating with the lower part of the Jamesoni Zone (Fig. 12, Table 2). This age is in agreement with the Pliensbachian age inferred for the *Eomiodon* Horizon (Posenato and Masetti, 2012; Posenato et al., 2013b) but is younger than the late Sinemurian age previously proposed for the FO of *O. primaeva* in the Rotzo Formation (Fugagnoli and Loriga Broglio, 1998; Fugagnoli, 2004) and in the Lower Jurassic Tethyan LBF schemes (e.g., Kabal and Tasli, 2003;Velić, 2007; Gale, 2014). These earlier interpretations were based on the Morocco successions, where the FO of *Orbitopsella primaeva* is placed between a level with middle Sinemurian ammonites and a level with middle lower-Pliensbachian ammonites (Septfontaine, 1984, fig. 4). It is evident that these chronostratigraphical constraints are compatible with the lower Pliensbachian age proposed

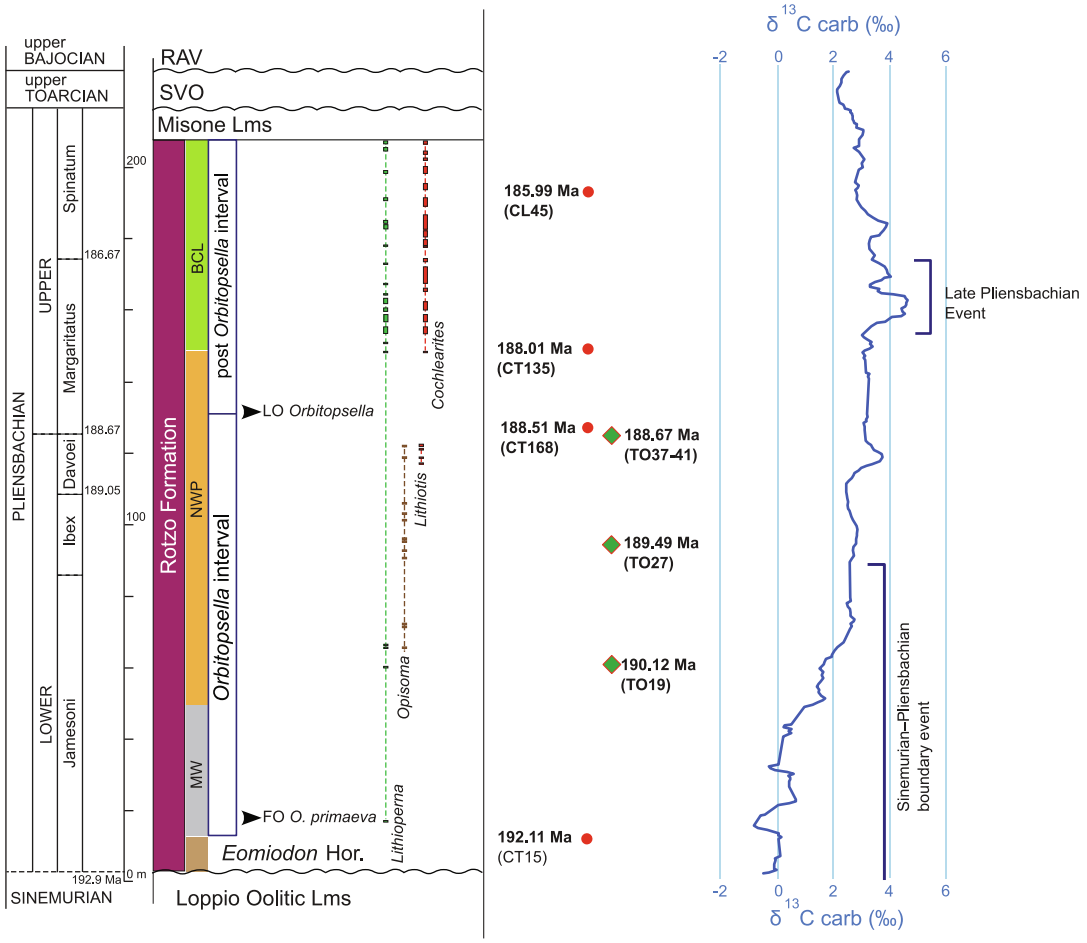

Fig. 12. Chronostratigraphical calibration of the biostratigraphical distribution of larger benthic foraminifera and lithiotid bivalves in the Toraro–Campoluzzo composite section. By integrating strontium isotope stratigraphy and carbon isotope stratigraphy we obtained a well-constrained framework for the correlation of the first occurrence (FO) of *Orbitopsella primaeva* with the lower part of the Jamesoni Zone and of the last occurrence (LO) of the genus *Orbitopsella* with the lowermost part of the Margaritatus Zone. This represent a significant refinement of the previously accepted ages which were poorly constrained by indirect correlation to ammonite-bearing beds. Similarly, we obtained new constraints on the ages of the onset, development, and demise of the most renowned bivalves of the *Lithiotis* Facies in the Rotzo Formation.

here through the integration of SIS and carbon isotope stratigraphy. A comparable age for the FO of *Orbitopsella* has also been reported in the Betic Cordillera (southern Spain; Gonzáles-Donoso et al., 1977).

In the TCs, the LO of the genus *Orbitopsella* (*Orbitopsella praecursor* and *Orbitopsella primaeva/precursor*) is in the upper part of NWP unit, at c. 130 m from the base of the section. The SIS ages of the brachiopod shells TO37–41 (from 120.4 m to 124.9 m from the base) and of the bulk sample CT168 (at 126.8 m from the base) constrain this level to the lowermost part of the upper Pliensbachian correlating with the Stokesi Subzone of the Margaritatus Zone (Fig. 12, Tables 1–2). Most studies on the biostratigraphy of Lower Jurassic LBF propose a slightly older age for the LO of the genus *Orbitopsella*, either in the uppermost lower Pliensbachian (uppermost Carixian in Septfontaine, 1984) or at the lower–upper Pliensbachian boundary (e.g. Bassoullet, 1997; Fugagnoli and Loriga Broglio, 1998; Kabal and Tasli, 2003; Fugagnoli, 2004; Velić, 2007). These earlier interpretations either rely on Septfontaine (1984) or do not provide explicit evidence. In fact, Septfontaine's (1984, p. 221) calibration of the LO of *Orbitopsella praecursor* to the lower Pliensbachian is based solely on correlation with levels containing the ammonite genus *Fuciniceras*. However, this genus is also typical in the lower upper Pliensbachian Stokesi Subzone (e.g., Meister et al., 2011) and the Fuciniceras lavinianum Zone is regarded as the Tethyan equivalent of the Stokesi Subzone (Braga, 1983; Braga et al., 1982, 2025). *Orbitopsella dubari*, exclusively identified in the lowermost upper Pliensbachian (Hottinger, 1967; Bassoullet, 1997), occurs associated with *O. praecursor* in the Rotzo Formation but not in the Monte Toraro area (Fugagnoli, 2004). The lowermost upper Pliensbachian age (Stokesi Subzone) proposed here for the LO of the genus *Orbitopsella* in the Rotzo Formation, constrained by SIS, is therefore entirely compatible with the Septfontaine's framework (Septfontaine, 1984). This age is also supported by the occurrence of an ammonite of the Stokesi Subzone in *O. praecursor*-bearing beds of Monte Baldo (western Trento Platform; Sarti and Ferrari, 1999).

Pseudocyclammina liasica, generally considered an upper Pliensbachian–lower Toarcian species that typically appears after the LO of *Orbitopsella praecursor* (Septfontaine, 1984; Bassoullet, 1997), in the Monte Toraro section co-occurs with *O. praecursor* in the lower Pliensbachian and disappears in the lowermost upper Pliensbachian.

The post-*Orbitopsella* interval, c. 75 m-thick, encompasses the upper part of the studied section, from the LO of *O. praecursor* in the NWP unit of the Rotzo Formation up to the Rotzo Formation–Misone Limestone boundary (Fig. 12). This interval is characterized by the occurrence of *Amijiella amiji*, *Everticyclammina praevirguliana*, *Haurania deserta*, *Palaeomayincina termieri*,?*Lituosepta* sp., and *Pseudocyclammina* sp. In addition, *Bosniella oenensis* and *Cymbriaella lorigae* have their FO in the uppermost part of the Rotzo Formation (Fig. 2). Based on the SIS constraints (Table 2) and on the identification of the Late Pliensbachian Event in the $\delta^{13}C$ curve of the TCs (Fig. 12), the post-*Orbitopsella* interval of the Rotzo Formation can be assigned to the lowermost upper Pliensbachian (Margaritatus Zone, Stokesi Subzone) through to the uppermost Pliensbachian (Spinatum Zone).

6.5.2. Age and distribution of the lithiotid bivalves in the Rotzo Formation

In the lowermost part of the studied succession lithiotid bivalves are rare. They appear in MW unit at c. 16 m from the base of the Rotzo Formation with small (c. 10 cm high) and thin shells of *Lithioperna* (Fig. 12). This first level can be assigned to the lowermost Pliensbachian, based on the SIS age of sample CT15 (Table 2), and correlated with the lower part of the Jamesoni Zone (Fig. 12). *Lithioperna* re-appears in the lower part of NWP unit at c. 60 m from the base of the Rotzo Formation with larger (c. 20 cm high) and thicker specimens. This level can be attributed to the lower Pliensbachian based on the SIS age of the brachiopod shells of sample TO19 (Fig. 12, Table 1), and correlated with the upper part of the Jamesoni Zone, within the Sinemurian–Pliensbachian Boundary Event of the $\delta^{13}C$ curve (Fig. 12). Few metres above, the bivalve association also includes *Opisoma.* The first appearance of *Lithiotis* is recorded at c. 115 m from the base of the Rotzo Formation, where this aberrant lithiotid species constitutes m-thick accumulations intercalated with brachiopod-rich beds (Brandolese et al., 2019; Bassi et al., 2024). The SIS age of the brachiopods of samples TO37–41 support an age for the *Lithiotis* beds close to the boundary between the Davoei and the Margaritatus zones (Fig. 12, Table 1). *Cochlearites* appears in the BCL unit, forming thick lens-shaped accumulations (bivalve mounds) together with *Lithioperna*, which are characteristic of the upper Rotzo Formation. The SIS age of sample CT135 indicates that *Cochlearites–Lithioperna* mounds correspond to a level within the upper Pliensbachian Margaritatus Zone (Fig. 12), close to the boundary between the Stokesi and Subnodosum subzones (Table 2). This correlation is reinforced by the interpretation of the Late Pliensbachian Event recorded in the $\delta^{13}C$ curve (Fig. 12).

Lithiotid bivalves disappear at the Rotzo Formation–Misone Limestone boundary. This stratigraphical level is correlated with the uppermost Pliensbachian Spinatum Zone, based on the SIS age of sample CL45, and its position above the Late Pliensbachian Event in the $\delta^{13}C$ curve (Fig. 12).

The biostratigraphical distribution of the lithiotid bivalves documented in the TCs, which represents the depocenter of the Rotzo Formation, can be traced across the Trento Platform (e.g., Rotzo stratigraphical section; Franceschi et al., 2014). In the condensed and more landward successions of the Lessini Mountains, where the stratigraphical hiatus between the Rotzo Formation and the Loppio Oolite Limestone is perhaps longer, thick *Lithioperna* accumulations appear at c. 8 m above the base of the Rotzo Formation (e.g., Vajo dell'Anguilla section; Posenato and Masetti, 2012, fig. 5). In the same area, *Lithiotis* appears at c. 10 m above the base of the Rotzo Formation, while the last *Lithiotis* specimens, associated with *Cochlearites,* occur at c. 30 m above base (Campodalbero stratigraphical section; Posenato and Masetti, 2012, fig. 5). In the western part of the Trento Platform (Viote stratigraphical section), toward the Lombardia Basin, the first bed of the Rotzo Formation contains an accumulation of *Pachygervillia*, a thick and large bivalve of the *Lithiotis* Facies, with broad geographical and stratigraphical distribution (Posenato and Crippa, 2023). In this section, the first *Lithioperna* accumulation occurs at c. 25 m above the base (Franceschi et al., 2014).

The stratigraphical and geographical distribution of the large bivalves of the *Lithiotis* Facies in the Rotzo Formation reflects both evolutionary changes linked to global environmental perturbations, recorded by the strong Pliensbachian variations in $\delta^{13}C$, and local environmental changes, related to the significant tectonic activity that affected the Trento Platform during the Early Jurassic (e.g., Masetti et al., 2012; Martinelli et al., 2017; Franceschi et al., 2019). Establishing a common stratigraphical framework to disentangle local and global (or at least Tethyan-wide) events in the evolutionary history of lithiotid bivalves remains challenging due not only to the scarcity of reliable chronostratigraphical constraints but also to the complex interplay of regional and global drivers. References to lithiotid taxa lacking field photographs of diagnostic oriented shell sections should be considered with great caution. Available data from the Trento Platform point to three main proliferation phases of the lithiotid bivalves. The earliest, in the middle Sinemurian, is represented by *Gervilleioperna* (Posenato et al., 2024). The second, documented in this paper, recorded in the Ibex and Davoei zones, after the negative CIE of the Sinemurian–Pliensbachian Boundary Event, is characterized by an assemblage dominated by *Lithioperna*, *Lithiotis*, and *Opisoma*, with subordinate *Gervilleioperna, Pachygervillia*, and *Pseudopachymytilus*. The third phase, characterized by the *Cochlearites–Lithioperna* association, is recorded during the upper Pliensbachian Margaritatus zone and starts with the onset of the positive CIE of the Late Pliensbachian Event (Fig. 12). This phase records the maximum proliferation of lithiotids, when they formed some metre-thick and several hundred-metre-wide bivalve mounds (Posenato and Masetti, 2012). In the Trento Platform, the disappearance of the lithiotids in the latemost late Pliensbachian is related to a local increase in

water depth recorded by the deposition of the Misone Limestone. In the Apennine Platform (Trecalli et al., 2012; Posenato et al., 2018), Morocco (Brame et al., 2019), and Chile (Aberhan and von Hillebrandt, 1999) the lithiotids reached the early Toarcian, when they underwent extinction during the biocalcification crisis (e.g., Trecalli et al., 2012; Brame et al., 2019; Posenato et al., 2024). Among the bivalves of the *Lithiotis* Facies only *Gervilleioperna, Opisoma*, and *Pachyrisma* survived to this mass extinction, extending into the Middle–Late Jurassic (Posenato et al., 2024).

7. Conclusions

In the Toraro–Campoluzzo area (Trento Platform, Southern Alps, western Tethyan margin), at the depocenter of the Rotzo Formation, the onset of lagoonal conditions is marked by the deposition of the *Eomiodon* Horizon, which unconformably overlies the platform margin facies of the Loppio Oolitic Limestone. Carbon and strontium isotope stratigraphy constrain this horizon to lowermost Pliensbachian, correlating with the lower Jamesoni Zone.

Integration of isotope stratigraphy with biostratigraphical data refines the chronostratigraphical framework for lituolid LBF and the onset, development and demise of the *Lithiotis* Facies in the Rotzo Formation. The results are summarized as follows:

1. In the studied area the first occurrence of *Orbitopsella primaeva* lies in the lowermost lower Pliensbachian Jamesoni Zone, younger than the late Sinemurian age commonly accepted in the most used biostratigraphical schemes. The last occurrence of *Orbitopsella praecursor* is in the lowermost upper Pliensbachian (lowermost Margaritatus Zone), also younger than previously accepted so far. This revised calibration, based on carbon and strontium isotope stratigraphy, represents a significant improvement over earlier calibrations, which were based on poorly constrained indirect correlations with ammonite-bearing beds.
2. *Lithioperna* first appears in the lower part of the lowermost Pliensbachian Jamesoni Zone, followed by *Opisoma* in the upper part of the Jamesoni Zone. *Lithiotis* first occurs near the boundary between the Davoei and the Margaritatus zones, forming m-thick accumulations intercalated with brachiopod beds. The final stage of the *Lithiotis* Facies is represented by the occurrence of thick *Cochlearites–Lithioperna* mounds within the Margaritatus and Spinatum zones. Lithiotid bivalves disappear at the Rotzo Formation–Misone Limestone boundary, in the uppermost Pliensbachian Spinatum Zone.

The scarcity of ammonite-dated horizons in Lower Jurassic shallow-water carbonate platforms continues to limit chronostratigraphical resolution. The approach applied here demonstrates that integrating strontium and carbon-isotope stratigraphy provides a powerful tool for refining LBF and Lithiotid bivalve biostratigraphy. Extending this methodology across carbonate platforms will help unravel the evolutionary history of these faunas and their relationship to climate change and global carbon cycle perturbations during the Early Jurassic.

Supplementary data to this article can be found online at https://doi.org/10.1016/j.palaeo.2025.113423.

CRediT authorship contribution statement

Renato Posenato: Writing – review & editing, Writing – original draft, Methodology, Investigation, Funding acquisition, Formal analysis, Data curation, Conceptualization. **Davide Bassi:** Writing – review & editing, Writing – original draft, Methodology, Investigation, Funding acquisition, Formal analysis, Data curation, Conceptualization. **Mariano Parente:** Writing – review & editing, Writing – original draft, Methodology, Investigation, Funding acquisition, Formal analysis, Data curation, Conceptualization. **Hideko Takayanagi:** Writing – review & editing, Writing – original draft, Methodology, Investigation, Formal analysis, Data curation. **Anna Cipriani:** Writing – review & editing, Writing – original draft, Methodology, Investigation, Formal analysis, Data curation. **Claudio Garbelli:** Writing – review & editing, Writing – original draft, Methodology, Investigation, Formal analysis, Data curation. **Andrea Montanaro:** Methodology, Investigation. **Yoshihiro Asahara:** Writing – review & editing, Writing – original draft, Methodology, Investigation, Formal analysis, Data curation. **Yasufumi Iryu:** Writing – review & editing, Writing – original draft, Methodology, Investigation, Funding acquisition, Formal analysis, Data curation.

Declaration of competing interest

The authors declare that they have no known competing financial interests or personal relationships that could have appeared to influence the work reported in this paper.

Acknowledgements

This study was supported by local research fund of the University of Ferrara (FAR 2020–2023 to D.B. and R.P.), by the JSPS KAKENHI (Grant-in-Aid for Scientific Research) Grant number 21K18642 and 23K25959 (to Y.I.). This work was partly supported by World Premier International Research Center Initiative (WPI), MEXT, Japan.

This paper is a scientific contribution of the project "Biota resilience to global change: biomineralization of planktic and benthic calcifiers in the past, present and future", funded by the grant PRIN 2017RX9XXXY to R.P., D.B., and M.P. We are grateful to Lucia Angiolini (Editor), Uwe Brand, Jozsef Palfy, Matias Reolid, and an anonymous reviewer for their helpful comments.

Data availability statement

All data are included in the manuscript and supplementary information files.

Taxonomic list of LBF, calcareous algal, bivalve, and brachiopod taxa mentioned in the text and figures, listed in alphabetical order.

LBF:
Agerella martana (Farinacci, 1959).
Amijiella amiji (Henson, 1948).
Bosniella oenensis (Gušić, 1977).
Cymbriaella lorigae (Fugagnoli, 1999).
Everticyclammina praevirguliana (Fugagnoli, 2000).
Haurania deserta (Henson, 1948).
Lituosepta compressa (Hottinger, 1967).
Lituosepta recoarensis (Cati, 1959).
Orbitopsella dubari (Hottinger, 1967).
Orbitopsella praecursor (von Gümbel, 1872).
Orbitopsella primaeva (Henson, 1948).
Paleomayncina termieri (Hottinger, 1967).
Pseudocyclammina liasica (Hottinger, 1967).
Calcareous algae:
Palaeodasycladus mediterraneus (Pia) (Pia, 1927).
Microproblematicum:
Thaumatoporella parvovesiculifera (Raineri) (Pia, 1927).
Bivalves:
Cochlearites loppianus (Tausch, 1890).
Eomiodon serradensis (Tausch, 1890).
Lithioperna scutata (Dubar, 1948).
Lithiotis problematica (Gümbel, 1871).
Opisoma excavatum (Boehm, 1884).
Brachiopods:
Lychnothyris rotzoana (von Schauroth, 1865).

References

Aberhan, M., von Hillebrandt, A., 1999. The bivalve *Opisoma* in the Lower Jurassic of northern Chile. Profil 16, 149–164.

Ahm, A.-S., Husson, J., 2022. Local and Global Controls on Carbon Isotope Chemostratigraphy. Cambridge University Press.

Allan, J.R., Matthews, R.K., 1982. Isotope signatures associated with early meteoric diagenesis. Sedimentology 29, 797–817.

Álvaro, M., Barnolas, A., Cabra, P., Comas-Rengifo, M.J., Fernández-López, S.R., Goy, A., 1989. El Jurásico de Mallorca (Islas Baleares). Cuad. Geol. Ibérica 13, 67–120.

Banner, J.L., 1995. Application of the isotope and trace element geochemistry of strontium to studies of diagenesis in carbonate systems. Sedimentology 42, 805–824.

Banner, J.L., Hanson, G.H., 1990. Calculation of simultaneous isotopic and trace element variations during water-rock interaction with applications to carbonate diagenesis. Geochim. Cosmochim. Acta 54, 3123–3137.

Barbieri, G., Grandesso, P., 2007. Note illustrative della Carta Geologica d'Italia alla scala 1:50.000. foglio 082 Asiago. APAT Servizio Geologico d'Italia, p. 13.

Bassi, D., Fugagnoli, A., Posenato, R., Scott, D.B., 2008. Testate amoebae from the Early Jurassic of the western Tethys, north-east Italy. Palaeontology 51 (6), 1335–1339.

Bassi, D., Posenato, R., Nebelsick, J.H., 2015. Paleoecological dynamics of shallow-water bivalve carpets from a Lower Jurassic lagoonal setting, Northeast Italy. Palaios 30, 758–770.

Bassi, D., Angiolini, L., Nebelsick, J.H., Posenato, R., 2024. Success and demise of exceptionally preserved terebratulide brachiopod accumulations in a Jurassic (early Pliensbachian) tropical lagoonal setting (Southern Alps, Italy): brachiopod response to environmental changes. Palaeogeogr. Palaeoclimatol. Palaeoecol. 648, 112262.

Bassoullet, J.P., 1997. Les grands foraminifères. In: Cariou, E., Hantzpergue, P. (Eds.), Biostratigraphie du Jurassique ouest-Européen et méditerranéen. Zonation parallèles et distribution des invertébrés et microfossiles, 17. Bull. Cent. Rech. Explor. Prod. Elf. Mém, pp. 293–304.

Bassoullet, J.P., Fares, F., 1969. Les Orbitopselles du Lias du Djebel Hafid (Algérie). Rev. Micropaleontol. 18, 3–14.

Bassoullet, J.P., Fourcade, E., Peybernès, B., 1985. Paléobiogéographie des grandes foraminifères benthiques des marges néo-téthysiennes au Jurassique et au Crétacé inférieur. Bull. Soc. Géol. Fr. 8 (5), 699–713.

Bassoullet, J.-P., Boutakiout, M., Ecahrfaoui, H., 1999. Deux nouveaux genres, *Palaeocyclammina* et *Ijdranella*, foraminifères (Textulariina) d'un niveau Liasique à *Orbitopsella praecursor* (Gümbel) du moyen Atlas (Maroc). Rev. Micropaleontol. 42, 213–230.

Beccarelli-Bauck, L., 1988. Unter- bismitteljurassische Karbonatformationen am Westrand der Trento Platform (Südalpen, Norditalien). Münchn. Geowiss. Abh. 13, 1–86.

Berti Cavicchi, A., Bosellini, A., Broglio Loriga, C., 1971. Calcari a *Lithiotis problematica* o Calcari a "*Lithiotis*"? Mem. Geopaleontol. Univ. Ferrara 3 (1), 41–53.

Boehm, G., 1884. Beiträge zur Kenntniss der Grauen Kalke in Venetien. Z. Dtsch. Geol. Ges. 36, 737–782.

Boomer, I., Whatley, R.C., Bassi, D., Fugagnoli, A., Broglio Loriga, C., 2001. An Early Jurassic oligohaline ostracod assemblage within the marine carbonate platform sequence of the Venetian Prealps, NE Italy. Palaeogeogr. Palaeoclimatol. Palaeoecol. 166, 331–344.

Bosellini, A., Broglio Loriga, C., 1971. I "Calcari Grigi" di Rotzo (Giurassico inferiore, Altopiano di Asiago) e loro inquadramento nella paleo-geografia e nella evoluzione tettonico-sedimentaria delle Prealpi Venete. Ann. Univ. Ferrara, Nuova Serie 9 (5/l), 1–61.

BouDagher-Fadel, M.K., 2018. Evolution and Geological Significance of Larger Benthic Foraminifera, 2nd ed. University College London Press, London, UK, p. 693.

BouDagher-Fadel, M.K., Bosence, D.W., 2007. Early Jurassic benthic foraminiferal diversification and biozones in shallow-marine carbonates of western Tethys. Senckenb. Lethaea 87, 1–39.

BouDagher-Fadel, M.K., Lord, A.R., 2002. Larger foraminifera of the Jurassic Western Neotethys Ocean. Archaeol. Hist. Lebanon 15, 87–94.

BouDagher-Fadel, M.K., Rose, E.P.F., Bosence, D.W.J., Lord, A.R., 2001. Lower Jurassic foraminifera and calcified microflora from Gibraltar, Western Mediterranean. Palaeontology 44, 601–621.

Bougeault, C., Pellenard, P., Deconinck, J.-F., Hesselbo, S.P., Dommergues, J.-L., Bruneau, L., Cocquerez, T., Laffont, R., Huret, E., Thibault, N., 2017. Climatic and palaeoceanographic changes during the Pliensbachian (Early Jurassic) inferred from clay mineralogy and stable isotope (C-O) geochemistry (NW Europe). Global Planet. Change 149, 139–152.

Braga, J.C., 1983. Ammonites del Domerense de las Zona Subbética (Cordilleras Béticas, Sur de España). PhD Thesis,. Universidad de Granada, Granada.

Braga, J.C., Comas-Rengifo, M.J., Goy, A., Rivas, P., 1982. Comparaciones faunísticas y correlaciones en el Pliensbachiense de la Zona Subbética y Cordillera Ibérica. Bol. Rev. R. Soc. Esp. Hist. Nat. 80, 221–244.

Braga, J.C., Sola, F., Comas-Rengifo, M.J., Bassi, D., 2025. The Lower to middle Jurassic of the Maláguide complex (Internal zones, Betic Cordillera, S Spain) in Sierra Cabrera (Almería) and Cerro de San Antón (Málaga). J. Iber. Geol. https://doi.org/10.1007/s41513-025-00301-0.

Brame, H.-M.R., Martindale, R.C., Ettinger, N.P., Debeljak, I., Vasseurc, R., Lathuilièrec, B., Kabiri, L., Bodin, S., 2019. Stratigraphic distribution and paleoecological significance of Early Jurassic (Pliensbachian-Toarcian) lithiotid-coral reefal deposits from the Central High Atlas of Morocco. Palaeogeogr. Palaeoclimatol. Palaeoecol. 514, 813–837.

Brand, U., Logan, A., Bitner, M.A., Griesshaber, E., Azmy, K., Buhl, D., 2011. What is the ideal proxy for Palaeozoic seawater chemistry? Mem. Ass. Australasian Palaeontol. 41, 9–24.

Brandolese, V., Posenato, R., Nebelsick, J.H., Bassi, D., 2019. Distinguishing core and flank facies based on shell fabrics in Lower Jurassic lithiotid shell beds. Palaeogeogr. Palaeoclimatol. Palaeoecol. 526, 1–12.

Broglio Loriga, C., Neri, C., 1976. Aspetti paleobiologici e paleogeografici della facies a '*Lithiotis*' (Giurese inf.). Riv. Ital. Paleontol. Strat. 82, 651–706.

Broglio Loriga, C., Posenato, R., 1996. Adaptive strategies of Lower Jurassic and Eocene multivincular bivalves. Boll. Soc. Paleontol. Ital. Spec. 3, 45–61.

Callomon, J.M., Cresta, S., Pavia, G., 1994. A revision of the classical Aalenian succession in the Middle Jurassic of S. Vigilio, Lake Garda, Northern Italy. Geobios Mem. Spec. 17, 103–110.

Castellarin, A., 1972. Evoluzione paleotettonica sinsedimentaria del limite tra "piattaforma veneta" e "bacino lombardo," a nord di Riva del Garda. Giorn. Geol. 38, 11–212.

Castellarin, A., Picotti, V., Cantelli, L., Claps, M., Trombetta, L., Selli, L., Carton, A., 2005. Note Illustrative della Carta Geologica D'Italia, foglio 080 Riva del Garda. APAT, Serv. Geol. It, Firenze, pp. 1–145.

Cati, F., 1959. Un nuovo lituolide nei Calcari Grigi liassici del vicentino. Giorn. Geol. 27, 1–10.

Chinzei, K., 1982. Morphological and structural adaptations to soft substrates in the Early Jurassic monomyarians *Lithiotis* and *Cochlearites*. Lethaia 15, 179–197.

Chiocchini, M., Mancinelli, A., 1977. Microbiostratigrafia del Mesozoico in facies di piattaforma carbonatica dei Monti Aurunci (Lazio Meridionale). St. Geol. Camerti 3, 109–152.

Chiocchini, M., Mancinelli, A., 1978. Ricerche geologiche sul Mesozoico del Gran Sasso d'Italia (Abruzzo). III. Correlazioni microbiostratigrafiche tra facies di margine della piattaforma carbonatica e facies pelagiche del Giurassico e Cretaceo inferiore. St. Geol. Camerti 4, 19–36.

Chiocchini, M., Mancinelli, A., Molinari-Paganelli, V., Tilia-Zuccari, A., 1979. Répartition stratigraphique des algues dasycladales et codiacées dans les successions Mésozoïques de plate-forme carbonatée du Lazio centre-méridional (Italie). Bull. Centre Rech. Explor. Prod. Elf-Aquitaine 3, 525–535.

Chiocchini, M., Farinacci, A., Mancinelli, A., Molinari, V., Protetti, M., 1994. Biostratigrafia e foraminiferi, dasicladacee e calpionelle delle successioni carbonatiche mesozoiche dell'Appennino Centrale (Italia). In: Mancinelli, A. (Ed.), Biostratigrafia dell'Italia Centrale. St. Geol, Camerti, Spec. Vol. (A), pp. 9–129.

Clari, P., 1975. Caratteristiche sedimentologiche e paleontologiche di alcune sezioni dei Calcari Grigi del Veneto. Mem. Ist. Geol. Mineral. Univ. Padova 31, 1–63.

Clari, P.A., Pavia, G., 2002. Stop 4. The Jurassic succession at the Cima Campo di Luserna Fortress. In: Santantonio, M. (Ed.), General field trip guidebook, 6th Int. Symposium on the Jurassic System. Palermo, pp. 289–291.

Clari, P.A., Marini, P., Pastorini, M., Pavia, G., 1984. Il Rosso Ammonitico Inferiore (Baiociano–Calloviano) nei Monti Lessini settentrionali (Verona). Riv. It. Paleont. Strat. 90, 15–86.

De Castro, P., 1962. Il Giura–Lias dei Monti Lattati e dei rilievi ad Ovest della Valle dell'Imo e della Piana di Montoro. Boll. Soc. Nat. Napoli 71, 1–34.

Dozet, S., 2009. Lower Jurassic carbonate succession between Predole and Mlačevo, Central Slovenia. RMZ 56, 164–193 (in Slovenian with English abstract).

Duarte, L.V., Comas-Rengifo, M.J., Silva, R.L., Paredes, R., Goy, A., 2014. Carbon isotope stratigraphy and ammonite biochronostratigraphy across the Sinemurian–Pliensbachian boundary in the western Iberian margin. Bull. Geosci. 89, 719–736.

Dubar, G., 1948. La faune domerienne du Lias marocain (domaine atlasique). In: Notes Mem. Serv. Géol. Maroc (Rabat), 68, p. 250.

Emrich, K., Ehhalt, D.H., Vogel, J.C., 1970. Carbon isotope fractionation during the precipitation of calcium carbonate. Earth Planet. Sci. Lett. 8, 363–371.

Farinacci, A., 1959. Le microbiofacies giurassiche dei Monti Martani. Ann. Univ. Roma, Ist. Geol. Paleontol. 8, 41, 1–60.

Flügel, E., 1983. Mikrofazies der Pantokrator-Kalke (Lias) von Korfu, Griechenland. Facies 8, 263–300.

Franceschi, M., Dal Corso, J., Posenato, R., Roghi, G., Masetti, D., Jenkyns, H.C., 2014. Early Pliensbachian (Early Jurassic) C-isotope perturbation and the diffusion of the Lithiotids Fauna: insights from the western Tethys. Palaeogeogr. Palaeoclimatol. Palaeoecol. 410, 255–263.

Franceschi, M., Dal Corso, J., Cobianchi, M., Roghi, G., Penasa, L., Picotti, V., Preto, N., 2019. Tethyan carbonate platform transformations during the Early Jurassic (Sinemurian–Pliensbachian, Southern Alps): comparison with the Late Triassic Carnian Pluvial Episode. GSA Bull. 13, 1255–1277.

Fraser, N.M., Bottjer, D.J., Fischer, A.F., 2004. Dissecting "*Lithiotis*" bivalves: implications for the Early Jurassic reef eclipse. Palaios 19, 51–67.

Frijia, G., Parente, M., Di Lucia, M., Mutti, M., 2015. Carbon and strontium isotope stratigraphy of the Upper Cretaceous (Cenomanian-Campanian) shallow-water carbonates of southern Italy: chronostratigraphic calibration of larger foraminifera biostratigraphy. Cretac. Res. 53, 110–139.

Fugagnoli, A., 1998. Le associazioni a foraminiferi bentonici del Giurassico Inferiore della Piattaforma di Trento (Calcari Grigi – Liassico). Sistematica, biostratigrafia e paleoecologia. Unpublished Ph.D. thesis,. Univ. Ferrara, p. 206.

Fugagnoli, A., 1999. Cymbriaella lorigae, a new foraminiferal genus (Textulariina) from the Early Jurassic of the Venetian Prealps (Northeastern Italy). Rev. Micropaléontol. 42 (2), 99–110.

Fugagnoli, A., 2000. First record of *Everticyclammina* Redmond 1964 (*E. praevirguliana* n. sp.; Foraminifera) from the Early Jurassic of the Venetian Prealps (Calcari Grigi, Trento platform, northern Italy). J. Foraminifer. Res. 30, 126–134.

Fugagnoli, A., 2004. Trophic regimes of benthic foraminiferal assemblages in Lower Jurassic shallow water carbonates from northeastern Italy (Calcari Grigi, Trento Platform, venetian Prealps). Palaeogeogr. Palaeoclimatol. Palaeoecol. 205, 111–130.

Fugagnoli, A., Bassi, D., 2015. Taxonomic and biostratigraphic reassessment of *Lituosepta recoarensis* Cati, 1959 (Foraminifera, Lituolacea). J. Foraminifer. Res. 45, 402–412.
Fugagnoli, A., Loriga Broglio, C., 1998. Revised biostratigraphy of Lower Jurassic shallow water carbonates from the venetian Prealps (Calcari Grigi, Trento Platform, Northern Italy). St. Trentini Sci. Nat. Acta Geologica 73 (1996), 35–73.
Fujioka, H., Suzuki, K., Takayanagi, H., Tasumi, E., Yamamoto, K., Ohfuji, H., Miyajima, T., Iryu, Y., 2025. Effects of artificial diagenetic alteration on the microstructure, isotopic composition, and metal element concentrations in brachiopod shells. Geochem. J. 59, 96–117. https://doi.org/10.2343/geochemj.GJ25005.
Gale, L., 2014. Lower Jurassic foraminiferal biostratigraphy of Podpeč Limestone (External Dinarides, Slovenia). Geologija 57, 119–146.
Gale, L., Kelemen, M., 2017. Early Jurassic foraminiferal assemblages in platform carbonates of Mt. Krim, Central Slovenia. Geologija 60, 99–115.
Garbelli, C., Angiolini, L., Jadoul, F., Brand, U., 2012. Micromorphology and differential preservation of Upper Permian brachiopod low-Mg calcite. Chem. Geol. 299, 1–10.
Geyer, O.F., 1977. Die "Lithiotis-Kalke" im Bereich der unterjurassischen Tethys. Neues Jahrb. Geol. Palaontol. Abh. 153 (3), 304–340.
Geyman, E.C., Maloof, A.C., 2021. Facies control on carbonate $\delta^{13}C$ on the Great Bahama Bank. Geology 49 (9), 1049–1054.
Gonzáles-Donoso, J.M., Linares, A., Rivas, P., 1974. El Lias inferior y medio de Poloria (serie del Zegri, Zona Subbética, norte de Granada). Estud. Geol. 30, 639–654.
Gonzáles-Donoso, J.M., Linares, A., Rivas, P., 1977. Sur la position stratigraphique du genre *Orbitopsella* dans le secteur central de chaînes bétiques. Actes 6th Coll. Africain de Micropaléont., Tunis 1974. Ann. Mines Géol. 28, 253–259.
Gradstein, F.M., Ogg, J.G., Schmitz, M.D., Ogg, G.M., 2020. The Geologic Time Scale 2020, 2. Elsevier, Amsterdam, p. 1357.
Gümbel, C.W., 1871. Die sogennanten Nulliporen, *Lithiotis problematica*. Abh. Königl. Bayer Akad. Wiss. Cl. 2 (1), 38–52.
Gušić, I., 1977. A new foraminiferal family Biokovinidae from the Jurassic of the Dinarids and its phylogenetic relationships. Palaeontol. Jugosl. 18, 1–31.
Gušić, I., Velić, I., 1978. *Lituolipora polymorpha* n. gen., n. sp. (Foraminiferida, Lituolacea?) from the middle Liassic of the Outer Dinarids in Croatia and the establishment of a new family. Lituoliporidae. Geol. Vjesnik 30, 73–93.
Halverson, G.P., Hoffman, P.F., Schrag, D.P., Maloof, A.C., Rice, H.N., 2005. Toward a Neoproterozoic composite carbon-isotope record. Geol. Soc. Am. Bull. 117, 1181–1207.
Han, Z., Hu, X., He, T., Newton, R.J., Jenkyns, H.C., Jamieson, R.A., Franceschi, M., 2022. Early Jurassic long-term oceanic sulfur-cycle perturbations in the Tibetan Himalaya. Earth Planet. Sci. Lett. 578, 117261.
Henson, F.R.S., 1948. Larger Imperforate Foraminifera of South-Western Asia. Families Lituolidae, Orbitolinidae and Meandropsinidae. British Museum (Nat. Hist.), London, p. 128.
Hesselbo, S.P., Jenkyns, H.C., Duarte, L.V., Oliveira, C.V., 2007. Carbon-isotope record of the Early Jurassic (Toarcian) Oceanic Anoxic Event from fossil wood and marine carbonate (Lusitanian Basin, Portugal). Earth Planet. Sci. Lett. 253, 455–470.
Hesselbo, S.P., Ogg, J.G., Ruhl, M., Hinnov, L.A., Huang, C.J., 2020. The Jurassic period. In: Gradstein, F.M., Ogg, J.G., Schmitz, M.D., Ogg, G.M. (Eds.), Geologic time scale 2020. Elsevier, pp. 955–1021.
Hottinger, L., 1967. Foraminifères imperforés du Mésozoïque marocain. Not. Mém. Serv. Gèol. Maroc. 209, 61–168.
Hottinger, L., 1978. Comparative anatomy of elementary shell structures in selected Larger Foraminifera. In: Hedley, R., Adams, C. (Eds.), Foraminifera, 3. Academic Press, London, pp. 203–266.
Hottinger, L., 2006. Illustrated glossary of terms used in foraminiferal research. Carnets Géol. Mém. 2006 (02), 1–126.
Huck, S., Heimhofer, U., Rameil, N., Bodin, S., Immenhauser, A., 2011. Strontium and carbon-isotope chronostratigraphy of Barremian–Aptian shoal-water carbonates: Northern Tethyan platform drowning predates OAE 1a. Earth Planet. Sci. Lett. 304, 547–558.
Hughes, G.W., 2018. A new thin-section based micropaleontological biozonation for the Saudi Arabian Jurassic carbonates. Micropaleontology 64, 331–364.
Immenhauser, A., Holmden, C., Patterson, W.P., 2008. Interpreting the carbon-isotope record of ancient shallow epeiric seas: Lessons from the recent. In: Pratt, B.R., Holmden, C. (Eds.), Dynamics of Epeiric Seas 48. Ass. Can. Spec. Publ, Geol, pp. 135–174.
Jenkyns, H.C., Clayton, C.J., 1986. Black shales and carbon isotopes in pelagic sediments from the Tethyan Lower Jurassic. Sedimentology 33, 87–106.
Kabal, Y., Tasli, K., 2003. Biostratigraphy of the Lower Jurassic carbonates from the Aydinick area (Central Taurides, S. Turkey) and morphological analysis of *Lituolipora termieri* (Hottinger, 1967). J. Foraminifer. Res. 33, 338–351.
Kaminski, M.A., 2004. The year 2000 classification of the agglutinated foraminifera. In: Bubik, M., Kaminski, M. (Eds.), Proceedings of the 6th International workshop agglutinated Foraminifera. Grzybowski Found. Spec. Pub, 8, pp. 237–255.
Korte, C., Hesselbo, S.P., 2011. Shallow marine carbon and oxygen isotope and elemental records indicate icehouse-greenhouse cycles during the Early Jurassic. Paleoceanography 26 (4), PA4219.
Lankester, E.R., 1885. Protozoa. In: Anon (Ed.), Encyclopaedia Britannica, 9th ed. vol. 19, pp. 830–866.
Loeblich Jr., A.R., Tappan, H., 1985. Some new and redefined genera and families of agglutinated foraminifera II. J. Foraminifer. Res. 15, 175–217.
Machel, H.G., 2000. Application of cathodoluminescence to carbonate diagenesis. In: Pagel, M., Barbin, V., Blank, P., Ohnenstetter, D. (Eds.), Cathodoluminescence in Geosciences. Springer, New York, pp. 271–301.
Maloof, A.C., Schrag, D.P., Crowley, J.L., Bowring, S.A., 2005. An expanded record of Early Cambrian carbon cycling from the Anti-Atlas Margin, Morocco. Can. J. Earth Sci. 42, 2195–2216.
Mancinelli, A., Chiocchini, M., Chiocchini, R.A., Romano, A., 2005. Biostratigraphy of Upper Triassic-Lower Jurassic carbonate platform sediments of the central-southern Apennines (Italy). Riv. Ital. Paleontol. Stratigr. 111, 271–283.
Marino, M., Santantonio, M., 2010. Understanding the geological record of carbonate platform drowning across rifted Tethyan margins: examples from the Lower Jurassic of the Apennines and Sicily (Italy). Sediment. Geol. 225, 116–137.
Martinelli, M., Franceschi, M., Massironi, M., Rizzi, A., Salvetti, G., Zampieri, D., 2017. An extensional syn-sedimentary structure in the Early Jurassic Trento Platform (Southern Alps) as analogue of potential reservoirs developing in rifting-affected carbonate platforms. Mar. Petrol. Geol. 79, 360–371.
Martire, L., 1992. Sequence stratigraphy and condensed pelagic sediments. An example from the Roso Ammonitico Veronese, northeastern Italy. Palaeogeogr. Palaeoclimatol. Palaeoecol. 94, 169–191.
Martire, L., 1996. Stratigraphy, facies and sedimentary tectonics in the Jurassic Rosso Ammonitico Veronese (Altopiano di Asiago, NE Italy). Facies 35, 209–236.
Martire, L., Clari, P., Lozar, F., Pavia, G., 2006. The Rosso Ammonitico Veronese (Middle–Upper Jurassic of the Trento Plateau): a proposal of lithostratigraphic ordering and formalization. Riv. It. Paleontol. Strat. 112, 227–250.
Masetti, D., Claps, M., Giacometti, A., Lodi, P., Pignatti, P., 1998. I Calcari Grigi della Piattaforma di Trento (Lias inferiore e Medio, Prealpi Venete). Atti Ticinesi Sci. Terra 40, 139–183.
Masetti, D., Fantoni, R., Romano, R., Sartorio, D., Trevisani, E., 2012. Tectonostratigraphic evolution of the Jurassic extensional basins of the eastern Southern Alps and Adriatic foreland based on an integrated study of surface and subsurface data. AAPG Bull. 96 (11), 2065–2089.
Masetti, D., Figus, B., Jenkyns, H.C., Barattolo, F., Mattioli, E., Posenato, R., 2017. Carbon-isotope anomalies and demise of carbonate platforms in the Sinemurian (Early Jurassic) of the Tethyan region: evidence from the Southern Alps (Northern Italy). Geol. Mag. 154 (3), 625–650.
McArthur, J.M., 1994. Recent trends in strontium isotope stratigraphy. Terra Nova 6, 331–358.
McArthur, J.M., Steuber, T., Page, K.N., Landman, N.H., 2016. Sr-isotope stratigraphy: assigning time in the Campanian, Pliensbachian, Toarcian, and Valanginian. J. Geol. 145, 569–586.
McArthur, J.M., Howarth, R.J., Shields, G.A., Zhou, Y., 2020. Strontium isotope stratigraphy. In: Gradstein, F.M., Ogg, J.G., Schmitz, M.D., Ogg, G.M. (Eds.), The Geologic Time Scale 2020. Elsevier, pp. 211–238.
Meister, C., Dommergues, J.-L., Dommergues, C., Lachkar, N., El Hariri, K., 2011. Les ammonites du Pliensbachien du jebel Bou Rharraf (Haut Atlas oriental, Maroc). Geobios 44, 117.e1–117.e60.
Mercuzot, M., Pellenard, P., Durlet, C., Bougeault, C., Meister, C., Dommergues, J.-L., Thibault, N., Baudin, F., Mathieu, O., Bruneau, L., 2019. Carbon-isotope events during the Pliensbachian (Lower Jurassic) on the African and European margins of the NW Tethyan Realm. Newsl. Stratigr. 53, 41–69.
Morettini, E., Santantonio, M., Bartolini, A., Cecca, F., Baumgartner, P., Hunziker, J., 2002. Carbon isotope stratigraphy and carbonate production during the Early–Middle Jurassic: examples from the Umbria–Marche–Sabina Kübler Apennines (central Italy). Palaeogeogr. Palaeoclimatol. Palaeoecol. 184, 251–273.
Nieto, L.M., Molina, J.M., Ruiz-Ortiz, P.A., Fraguas, Á., Reolid, M., 2023. Evolution from carbonate platform to pelagic environments in the south Iberian paleomargin (Pliensbachian–early Toarcian, Early Jurassic): carbonate features and isotope geochemistry. Minerals 13 (11), 1386. https://doi.org/10.3390/min13111386.
Okai, T., Suzuki, A., Terashima, S., Inoue, M., Nohara, M., Kawahata, H., Imai, N., 2004. Collaborative analysis of GSJ/AIST geochemical reference materials JCp-1 (coral) and JCt-1 (giant clam). Chikyukagaku (Geochemistry) 38, 281–286 (in Japanese with English abstract). 10.14934/chikyukagaku.38.281.
Parente, M., Frijia, G., Di Lucia, M., 2007. Carbon-isotope stratigraphy of Cenomanian–Turonian platform carbonates from southern Apennines (Italy): a chemostratigraphic approach to the problem of correlation between shallow-water and deep-water successions. J. Geol. Soc. London 164, 609–620.
Patterson, W.P., Walter, L.M., 1994. Depletion of ^{13}C in seawater ΣCO_2 on modern carbonate platforms: significance for the carbon isotope record of carbonates. Geology 22, 885–888.
Peti, L., Thibault, N., Clémence, M.-E., Korte, C., Dommergues, J.-L., Bougeault, C., Pellenard, P., Jelby, M.E., Ullmann, C.V., 2017. Sinemurian–Pliensbachian calcareous nannofossil biostratigraphy and organic carbon isotope stratigraphy in the Paris Basin: calibration to the ammonite biozonation of NW Europe. Palaeogeogr. Palaeoclimatol. Palaeoecol. 468, 142–161.
Petti, F.M., Bernardi, M., Todesco, R., Avanzini, M., 2011. Dinosaur footprints as ultimate evidence for a terrestrial environment in the late Sinemurian Trento Carbonate Platform. Palaios 26, 601–606.
Pia, J., 1927. Thallophyta. In: Hirmer, M. (Ed.), Handbuch der Paläobotanik, 1. R. Oldenbourg, Munich and Berlin, pp. 31–136.
Posenato, R., Crippa, G., 2023. *Pachygervillia anguillaensis* new genus and new species: a bivalve of the Lower Jurassic *Lithiotis* facies and insight on the systematics of the Plicatostylidae. Riv. Ital. Paleontol. Stratigr. 129 (3), 551–572.
Posenato, R., Masetti, D., 2012. Environmental control and dynamics of Lower Jurassic bivalve build-ups in the Trento Platform (Southern Alps, Italy). Palaeogeogr. Palaeoclimatol. Palaeoecol. 361–362, 1–13.
Posenato, R., Bassi, D., Nebelsick, J., 2013a. *Opisoma excavatum* Bohem, a Lower Jurassic alatoform chambered bivalve. Lethaia 46, 242–437.
Posenato, R., Bassi, D., Avanzini, M., 2013b. Bivalve pavements from shallow-water black-shales in the Early Jurassic of northern Italy: a record of salinity- and oxygen-

depleted environmental evolutionary dynamics. Palaeogeogr. Palaeoclimatol. Palaeoecol. 369, 262–271.
Posenato, R., Bassi, D., Trecalli, A., Parente, M., 2018. Taphonomy and evolution of Lower Jurassic lithiotid bivalve accumulations in the Apennine Carbonate Platform (southern Italy). Palaeogeogr. Palaeoclimatol. Palaeoecol. 489 (1), 261–271.
Posenato, R., Crippa, G., de Winter, N.J., Frijia, G., Kaskes, P., 2022. Microstructures and sclerochronology of exquisitely preserved Lower Jurassic lithiotid bivalves: paleobiological and paleoclimatic significance. Palaeogeogr. Palaeoclimatol. Palaeoecol. 602, 111162.
Posenato, R., Crippa, G., de Winter, N.J., Claeys, P., Godreis, S., Frijia, G., Brombin, V., 2024. Microstructures and sclerochronology of the *Lithiotis* Facies bivalves (Lower Jurassic): paleobiological and paleoclimatic significance and their resilience to the early Toarcian extinction. Palaeogeogr. Palaeoclimatol. Palaeoecol. 649, 112329.
Preto, N., Breda, A., Dal Corso, J., Franceschi, M., Rocca, F., Spada, C., Roghi, G., 2017. The Loppio Oolitic Limestone (Early Jurassic, Southern Alps): a prograding oolitic body with high original porosity originated by a carbonate platform crisis and recovery. Mar. Petrol. Geol. 79, 394–411.
Prokoph, A., Shields, G.A., Veizer, J., 2008. Compilation and time-series analysis of marine carbonate $\delta^{18}O$, $\delta^{13}C$, $^{87}Sr/^{86}Sr$ and $\delta^{34}S$ databases through Earth history. Earth Sci. Rev. 87, 113–133.
Romanek, C.S., Grossman, E.L., Morse, J.W., 1992. Carbon isotopic fractionation in synthetic aragonite and calcite: effects of temperature and precipitation rate. Geochim. Cosmochim. Acta 56, 419–430.
Ruiz-Ortiz, P.A., Bosence, D.W.J., Rey, J., Nieto, M., Castro, J.M., Molina, J.M., 2004. Tectonic control of facies architecture, sequence stratigraphy and drowning of a Liassic carbonate platform (Betic Cordillera, Southern Spain). Basin Res. 16, 235–257.
Sarti, C., Ferrari, G., 1999. The first record of an in situ ammonite from the upper part of the Calcari Grigi di Noriglio Formation of the Monte Baldo (Trentino, Northern Italy). Neues Jahrb. Geol. Paläontol. 213 (3), 313–334.
Sartoni, S., Crescenti, U., 1959. La zona a *Palaeodasycladus* (Pia) nel Lias dell'Appennino meridionale. Giorn. Geol. 27, 115–139.
Sartoni, S., Crescenti, U., 1962. Ricerche biostratigrafiche nel Mesozoico dell'Appennino meridionale. Giorn. Geol. 29, 162–302.
Schlagintweit, F., 1991. On the occurrence of *Amijiella amiji* (Foraminifera) in the Tithonian–Berriasian of the Lerchkogel Limestone (Northern Calcareous Alps/Austria). Rev. Paléobiol. 10, 247–253.
Schlagintweit, F., Velić, I., 2011. Foraminiferan test and dasycladalean thalli as cryptic microhabitats for thaumatoporellacean algae from Mesozoic (Late Triassic–Late Cretaceous) platform carbonates. Facies 58, 79–94.
Schoepfer, S.D., Algeo, T.J., van de Schootbrugge, B., Whiteside, J.H., 2022. The Triassic–Jurassic transition – a review of environmental change at the dawn of modern life. Earth Sci. Rev. 232, 104099.
Schöllhorn, I., Adatte, T., Houben, A., Van de Schootbrugge, B., Charbonnier, G., Janssen, N., Föllmi, K.B., 2020. Climate and environmental response to the break-up of Pangea during the Hettangian–Pliensbachian; the Dorset coast (UK) revisited. Global Planet. Change 185, 103096.
Schootbrugge van de, B., Bailey, T.R., Rosenthal, Y., Katz, M.E., Wright, J.D., Miller, K. G., Feist-Burkhardt, S., Falkowski, P.G., 2005. Early Jurassic climate change and the radiation of organic-walled phytoplankton in the Tethys Ocean. Paleobiology 31, 73–97.
Schootbrugge van de, B., Harazim, D., Sorichter, K., Oschmann, W., Fiebig, J., Püttmann, W., Peinl, M., Zanella, F., Teichert, B.M.A., Hoffmann, J., Stadnitskaia, A., Rosenthal, Y., 2010. The enigmatic ichnofossil *Tisoa siphonalis* and widespread authigenic seep carbonate formation during the Late Pliensbachian in southern France. Biogeosciences 7, 3123–3138.
Septfontaine, M., 1981. Les foraminifères imperforés des milieux de plate-forme au Mésozoïque, détermination practique, interprétation phylogénétique et utilisation biostratigraphique. Rev. Micropaleontol. 23, 169–203.
Septfontaine, M., 1984. Biozonation (a l'aide des foraminifères imperforés) de la plate-forme interne carbonatée liasique du Haut Atlas (Maroc). Rev. Micropaléont. 27, 209–229.
Septfontaine, M., 1985. Milieux de dépôts et foraminifères (Lituolidés) de la plate-forme carbonatée du Lias moyen au Maroc. Rev. Micropaléont. 28, 265–289.
Septfontaine, M., 1988. Vers une classification évolutive des Lituolidés (Foraminifères) Mésozoiques en milieu de plateforme carbonatée. Rev. Paléobiol. 2, 229–256.
Septfontaine, M., 2020. Chapter 8. Steps of morphogenesis and iterative evolution of imperforate larger foraminifera in shallow carbonate shelves during Mesozoic times: Possible relations to symbiotic and abiotic factors. In: Guex, J., et al. (Eds.), Morphogenesis, Environmental Stress and Reverse. Switzerland, Springer Nature, pp. 129–173.
Septfontaine, M., Arnaud-Vanneau, A., Bassoullet, J.P., Gusic, Y., Ramalho, M., Velić, I., 1991. Les foraminifères imperforeé des plates-formes carbonatées jurassiques: état des connaissances et perspectives d'avenir. Bull. Soc. Vaudoise Sci. Nat. 80, 255–277.
Sevillano, A., Septfontaine, M., Rosales, I., Barnolas, A., Badenas, B., Lopez-Garcia, J.-M., 2020. Lower Jurassic benthic foraminiferal assemblages from shallow marine platform carbonates of Mallorca (Spain): stratigraphic implications. J. Iber. Geol. 46, 77–94.
Simmons, M.D., 2020. Larger benthic foraminifera. Subchapter 3H. In: Gradstein, F.M., Ogg, J.G., Schmitz, M.D., Ogg, G.M. (Eds.), The Geologic Time Scale 2020. Elsevier, Amsterdam, pp. 88–98.
Sokač, B., 2001. Lower and middle Liassic calcareous algae (Dasycladales) from Mt. Velebit (Croatia) and Mt. Trnovski Gozd (Slovenia) with particular reference to the genus *Palaeodasycladus* (Pia, 1920) 1927 and its species. Geol. Croatica 54 (2), 133–257.
Speranza, F., Parisi, G., 2007. High-resolution magnetic stratigraphy at Bosso Stirpeto (Marche, Italy): anomalous geomagnetic field behavior during early Pliensbachian (Early Jurassic) times? Earth Planet Sci. Lett. 256, 344–359.
Storm, M.S., Hesselbo, S.P., Jenkyns, H.C., Ruhl, M., Ullmann, C.V., Xu, W., Leng, M.J., Riding, G.B., Gorbanenko, O., 2020. Orbital pacing and secular evolution of the Early Jurassic carbon cycle. PNAS 117 (8), 3974–3982.
Swart, P.K., 2008. Global synchronous changes in the carbon isotopic composition of carbonate sediments unrelated to changes in the global carbon cycle. Proc. Natl. Acad. Sci. U. S. A. 105, 13741–13745.
Swart, P.K., 2015. The geochemistry of carbonate diagenesis: the past, present and future. Sedimentology 62, 1233–1304.
Swart, P.K., Reijmer, J.J.G., Otto, R., 2009. A reevaluation of facies on Great Bahama Bank II: Variations in the $\delta^{13}C$, $\delta^{18}O$ and mineralogy of surface sediments. In: Swart, P.K., Eberli, G.P., McKenzie, J.A. (Eds.), Perspectives in Carbonate Geology. I. A.S. Spec, Publ, vol. 41. Blackwell, Oxford, pp. 47–59.
Tausch, L., 1890. Zur Kenntnis der Fauna der "Grauen Kalke". Abh. K.-K. Geol. Reich. 15 (2), 1–40.
Trecalli, A., Spangenberg, J., Adatte, T., Föllmi, K.B., Parente, M.J.E., Letters, P.S., 2012. Carbonate platform evidence of ocean acidification at the onset of the early Toarcian oceanic anoxic event. Earth Planet. Sci. Lett. 357, 214–225.
Veizer, J., Compston, W., 1974. $^{87}Sr/^{86}Sr$ composition of sea-water during the Phanerozoic. Geochim. Cosmochim. Acta 56, 431–443.
Veizer, J., Prokoph, A., 2015. Temperatures and oxygen isotopic composition of Phanerozoic oceans. Earth Sci. Rev. 146, 92–104.
Velić, I., 2007. Stratigraphy and palaeobiogeography of Mesozoic benthic foraminifera of the Karst Dinarides (SE Europe). Geol. Croat. 60, 1–113.
Voloshinova, N.A., 1958. On new systematics of the Nonionidae. Microfauna of the USSR. Proc. Oil Res. Geol. Inst. (VNIGRI) 115, 117–191.
von Gümbel, C.W., 1872. Über zwei jurassische Vorläufer des Foraminiferen-Geschlechtest *Nummulina* and *Orbitulites*. N. Jahr. Min. Geol. Paläont. 241–260.
von Schauroth, C., 1865. Verzeichniss der Versteinerungen im Herzogl. In: Naturaliencabinet zu Coburg (No. 1-4328): mit Angabe der Synonymen und Beschreibung vieler neuen Arten. Coburg, Verzeichniss der Versteinerungen im Herzog, pp. 1–327.
Winterer, H., Bosellini, A., 1981. Subsidence and sedimentation on Jurassic passive continental margin, southern Alps, Italy. Am. Assoc. Pet. Geol. Bull. 42, 394–419.
Woodfine, R.G., Jenkyns, H.C., Sarti, M., Baroncini, F., Violante, C., 2008. The response of two Tethyan carbonate platforms to the early Toarcian (Jurassic) oceanic anoxic event: environmental change and differential subsidence. Sedimentology 55, 1011–1028.
Yamamoto, K., Takizawa, M., Takanayagi, H., Asami, R., Iryu, Y., 2017. Nonlinear relationship between preservation of microstructure and geochemical composition of Pleistocene brachiopod shells from the Ryukyu Islands, southwestern Japan. Island Arc 26, e12217.